HHS Public Access

Author manuscript

*Kidney Int*. Author manuscript; available in PMC 2020 July 01.

Published in final edited form as:

*Kidney Int*. 2019 July ; 96(1): 139–158. doi:10.1016/j.kint.2019.02.014.

# The motor protein Myo1c regulates transforming growth factor-β-signaling and fibrosis in podocytes

**Ehtesham Arif**[1], **Ashish K. Solanki**[1], **Pankaj Srivastava**[1], **Bushra Rahman**[1], **Brian R Tash**[2], **Lawrence B Holzman**[2], **Michael G Janech**[1,5], **René Martin**[3], **Hans-Joachim Knölken**[3], **Wayne R. Fitzgibbon**[1], **Peifeng Deng**[1], **Milos N. Budisavljevic**[1], **Wing-Kin Syn**[4], **Cindy Wang**[4], **Joshua H. Lipschutz**[2], **Sang-Ho Kwon**[6], and **Deepak Nihalani**[1,*]

[1]Department of Medicine, Nephrology Division, Medical University of South Carolina, Charleston, South Carolina, USA.

[2]Department of Medicine, Renal Electrolyte and Hypertension Division, University of Pennsylvania, Philadelphia

[3]Department of Chemistry, TU Dresden, Dresden, Germany

[4]Department of Gastroenterology & Hepatology, Medical University of South Carolina, Charleston, South Carolina, USA.

[5]College of Charleston, Charleston, SC, USA.

[6]Department of Cellular Biology and Anatomy, Augusta University, Augusta, GA, USA.

## Abstract

Transforming growth factor-β (TGF-β) is known to play a critical role in the pathogenesis of many progressive podocyte diseases. However, the molecular mechanisms regulating TGF-β signaling in podocytes remain unclear. Using a podocyte-specific Myo1c knockout, we demonstrate whether Myo1c is critical for TGF-β-signaling in podocyte disease pathogenesis. Specifically, podocyte-specific Myo1c knockout mice were resistant to fibrotic injury induced by Adriamycin or nephrotoxic serum. Further, loss of Myo1c also protected from injury in the TGF-β-dependent unilateral ureteral obstruction mouse model of renal interstitial fibrosis. Mechanistic analyses showed that loss of Myo1c significantly blunted TGF-β signaling through downregulation of canonical and non-canonical TGF-β pathways. Interestingly, nuclear rather than

*Corresponding author: Deepak Nihalani, Ph. D, Associate Professor of Medicine, Smart State Chair, Medical University of South Carolina, Drug Discovery Building, DD514, 70 President St., Charleston, SC 29425, Phone: (843)876-2372, Fax: (843)879-5521.

AUTHOR CONTRIBUTIONS

EA, AKS, PS, BR, TBR, WRF, PF, CW and DN conducted the experiments and analyzed data. EA and DN generated the mouse strains. LBH, MGJ, RM, HJK, JHL and WKS provided critical reagents and helped with experimental designs. SHK performed RNASeq analysis and interpretation. MNB provided human kidney biopsy samples. EA and DN designed the experiments, interpreted data, and wrote the manuscript. All authors discussed results and commented on the manuscript.

CONFLICT OF INTEREST

The authors declare no conflict of interest.



Supplementary information is available at Kidney International's website: www.kidney-international.org.

the cytoplasmic Myo1c was found to play a central role in controlling TGF-β signaling through transcriptional regulation. Differential expression analysis of nuclear Myo1c associated gene promoters showed that nuclear Myo1c targeted the TGF-β responsive gene GDF-15, and directly bound to the GDF-15 promoter. Importantly, GDF15 was found to be involved in podocyte pathogenesis, where GDF15 was upregulated in glomeruli of patients with focal segmental glomerulosclerosis. Thus, Myo1c-mediated regulation of TGF-β responsive genes is central to the pathogenesis of podocyte injury. Hence, inhibiting this process may have clinical application in treating podocytopathies.

## Graphical Abstract

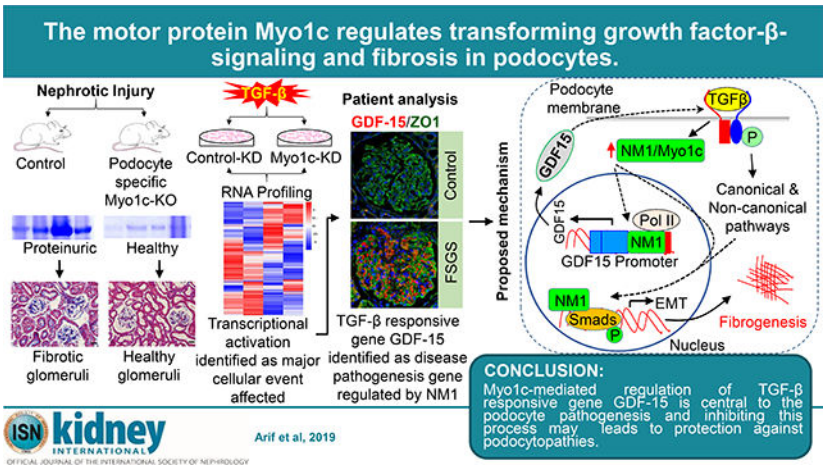


### Keywords

Fibrosis; Focal segmental glomerulosclerosis; Glomerulonephritis; Podocyte; TGF-beta; Glomerulus

## INTRODUCTION

Podocytes are the primary target of injury in many glomerular diseases, including minimal change, FSGS (focal and segmental glomerulosclerosis), membranous glomerulopathy, diabetes mellitus, and lupus nephritis.[1,2] While many reports describe the progression of injury in podocytes, which is characterized by significant changes to podocyte actin cytoskeleton leading to podocyte effacement and dysfunction,[2–4] the mechanisms that regulate this process are poorly understood. Over the years, with the identification of podocyte proteins and advancement in podocyte specific knockout studies several mechanisms have been highlighted that participate in the progression of podocyte damage. Many of these mechanisms involve activation of multiple signaling cascades, which control podocyte actin dynamics and podocytes response to injury.[4,5] TGF- β signaling is one of the prominent mechanisms that induces Smad dependent and independent pathway leading to fibrotic injury in glomerulus, which progresses to FSGS.[6–8] TGF-β is a pleiotropic cytokine that acts as a profibrotic stimulus and accumulates in various chronic renal diseases and experimental animal models[6,9] leading to progressive loss of renal function.[6,9] Despite its

critical role in podocyte disease pathogenesis, how this pathway is regulated in podocytes remains unknown. In this study, we demonstrate a novel role for the motor protein Myo1c as a transcriptional regulator of TGF-β responsive genes, thereby regulating the physiological effects of TGF-β signaling.

Class I myosins include myosins Myo1 A-H[10,11] and are actin-based molecular motors that actively participate in various cellular functions including intracellular trafficking, cell adhesion, motility and maintenance of membrane tension.[12–14] While significant structural homology exists between these myosins, they are expected to be involved in distinct physiological functions. Among these, Myo1c, which is a widely expressed motor protein, has been implicated in regulating hearing and glucose metabolism in humans.[11,14–16] In mice, the Myo1c gene produces two isoforms that are commonly referred as cytoplasmic and nuclear Myo1c.[17] The nuclear isoform (NM1) differs from cytoplasmic isoform (Myo1c) by the presence of 16 additional amino acids at the N- terminus. Cytoplasmic Myo1c has been shown to interact with various proteins, including Glut-4, and phosphoinositides, and these interactions participate in cellular functions such as generation of membrane tension, intracellular trafficking, cell migration, and signal transduction.[14,18,19] In contrast, the NM1 is involved in chromatin remodeling, transcription by all three RNA polymerases, mRNA maturation, and chromosome movement.[20–22] Recently another nuclear isoform of myo1c was identified, which is primarily present in humans and was undetectable in mice and contains additional 35 amino acids at the N-terminus of NM1.[22] In addition to increasing the kinetic diversity, this isoform was shown to affect the specific nucleotide-binding properties of Myo1c.[22] Collectively, these studies with different Myo1c isoforms suggest multiple functional roles for Myo1c, where in addition to regulating diverse cytoplasmic cellular events, it may participate in transcriptional regulation.

While the exact physiological role for Myo1c remains unknown, majority of studies have focused on biochemical characterization of Myo1c and its isoforms,[14,22,23] and have provided little information about the tissue-specific biological function of Myo1c. These findings further necessitate the need for a conditional mouse model of Myo1c, where all Myo1c isoforms can be genetically deleted in a tissue-specific fashion. In this study, using a podocyte-specific Myo1c knockout mouse model, we demonstrate a novel role for Myo1c as a regulator of TGF-β-induced fibrosis.

## RESULTS

### Selective deletion of Myo1c in mouse podocytes:

To understand the physiological function of Myo1c in podocytes, we generated podocyte specific Myo1c knockout mice using the Cre-lox system (Figure 1A).[24] A detailed list of construct validation procedures are listed in the supplemental results section (Figure S1 and Table S1). To confirm cre- mediated Myo1c excision, primary kidney cells from Myo1c$^{fl/fl}$ mice were treated with either Adeno-Cre or β-gal viruses. Western blot analysis showed loss of Myo1c protein in Adeno-Cre viruses treated cells (Figure S2A). The glomeruli isolated from Myo1c$^{fl/fl}$ and Myo1c$^{fl/fl}$pod-Cre$^{Tg/+}$ mice were subjected to qPCR analyses using specific Myo1c and its nuclear isoform [NM1(N16)] primers. The results showed significantly reduced expression of Myo1c and NM1(N16) in Myo1c$^{fl/fl}$pod-Cre$^{Tg/+}$

glomeruli, when compared to the Myo1c$^{fl/fl}$ glomeruli (Figure S2B). Loss of Myo1c from podocytes was confirmed by two independent procedures; the first approach used indirect immunofluorescence staining of kidney sections using Myo1c and NM1 antibodies. While Myo1c and NM1 were deleted in mouse podocytes, they were still present in mesangial cells (Figure 1B &C and figure S2C). To further confirm *Myo1c* deletion in mouse podocytes, Myo1c$^{fl/fl}$pod-Cre$^{Tg/+}$ mice were crossed with reporter mice (Gt(ROSA)26Sortm4(ACTB-tdTomato,-EGFP)Luo/J) that selectively labeled podocytes with green fluorescence[25]. The green podocytes were isolated by FACS sorting (Figure D&E and figure S2D&E) and subjected to qPCR analysis, which showed more than 90% reduction of both Myo1c isoforms (Figure. 1F). Collectively, these results confirmed genetic deletion of Myo1c in podocytes.

## Podocyte-specific genetic deletion of Myo1c protects mice from acute and chronic glomerular injuries.

Since Myo1c$^{fl/fl}$pod-Cre$^{Tg/+}$ mice displayed no phenotypic abnormalities even after aging, we wanted to investigate, whether loss of Myo1c changes their susceptibility towards glomerular injury. Therefore, we tested the response of these mice towards acute (NTS) and chronic (adriamycin) models of glomerular injuries.[26,27]

**a. Adriamycin-induced podocytopathy:** Adriamycin-induced nephropathy is a well-established rodent model of chronic kidney disease characterized by heavy proteinuria and injury to podocytes.[18,27,28] It is important to note that the Myo1c$^{fl/fl}$pod- Cre$^{Tg/+}$ mice were generated on C57BL/6N background that is genetically distinct from the widely used C57BL/6J mouse strain,[27] and are sensitive to adriamycin.[27] Thus, 10–12 week old mice were injected with either adriamycin or saline[27,29] (Figure 2A). Urine samples analyses showed induction of albuminuria in Myo1c$^{fl/fl}$ control mice at 3–4 weeks, whereas albuminuria was significantly attenuated in the Myo1c$^{fl/fl}$pod-Cre$^{Tg/+}$ mice (Figure 2B and C & Figure S3). The albuminuria in control mice was accompanied with significant podocyte foot process effacement as evaluated by SEM and TEM analyses (Figure 2D-F), which is consistent with adriamycin-induced injury.[27,28] Further quantitative analysis of electron micrographs showed that in comparison to Myo1c$^{fl/fl}$pod-Cre$^{Tg/+}$ mice, the numbers of slit-diaphragm (per area) were significantly decreased in the control mice (Figure 2E). Since slit diaphragm was preserved in Myo1c$^{fl/fl}$pod-Cre$^{Tg/+}$ mice, we next evaluated if loss of Myo1c also prevents injury- induced redistribution and loss of slit diaphragm proteins Nephrin and Neph1,[3,32–34] which are critical for podocyte development.[30,31] Thus, kidney sections from adriamycin- injured control and Myo1c$^{fl/fl}$pod-Cre$^{Tg/+}$ mice were analyzed by immunofluorescence using Neph1, Nephrin and Synaptopodin antibodies. While Neph1 and Nephrin expression was significantly reduced in podocytes of adriamycin treated control mice, the expression of these proteins was preserved in Myo1c$^{fl/fl}$pod-Cre$^{Tg/+}$ mice podocytes (Figure S4). The quantitative analyses showed that in comparison to adriamycin treated Myo1c$^{fl/fl}$pod-Cre$^{Tg/+}$ mice, Neph1 and Nephrin levels in control Myo1c$^{fl/fl}$ mice were reduced by ~67% and ~39% respectively (Figures S4C-D). Collectively, these results suggest that mice with podocyte-specific deletion of Myo1c are resistant to adriamycin- induced nephropathy.

**b. NTS-induced podocytopathy:** To test whether the observations made in the chronic adriamycin model of injury can be extended to an acute podocyte injury model, we used NTS model of podocytopathy in mice[35,36] (Figure 3A). The administration of NTS in control Myo1c$^{fl/fl}$ mice resulted in a remarkable increase in albuminuria within 24h, which persisted beyond 48h (for 5 days, figure S5), whereas the injection of control sheep IgG had no effect (Figure 3B-C). Further analysis of kidney sections by SEM and TEM showed increased foot process effacement characterized by flattening and fusion of the podocyte foot processes and loss of slit diaphragm (Figure 3D-F). In contrast, the parallel analysis of NTS-treated Myo1c$^{fl/fl}$pod-Cre$^{Tg/+}$ mice showed no albuminuria, no significant change in podocyte morphology, and well preserved slit diaphragm structures (Figure 3). Similar results were obtained on a FVB genetic background (Figure S5), further confirming this as a strain independent effect. Thus, podocyte- specific deletion of Myo1c in mice induces resistant towards glomerular injury induced by adriamycin and NTS.

## Podocytes specific deletion of Myo1c attenuated fibrosis in mice models of glomerulopathy.

Both, NTS and adriamycin injury models are characterized by the development of fibrotic lesions in glomeruli that define the extent of glomerular damage.[37, 38] To test if attenuation of adriamycin-induced glomerular injury in Myo1c$^{fl/fl}$pod-Cre$^{Tg/+}$ mice was associated with reduced fibrosis, kidney sections from these and control mice were stained with masson's trichrome and Sirius-red to assess the extent of fibrosis. The staining analysis of collagen deposits showed significant glomerular fibrosis in adriamycin treated control mice, which accounted for 20–24% of total glomerular area (Figure 4A-D). In contrast, Myo1c$^{fl/fl}$pod-Cre$^{Tg/+}$ mice had fewer collagen deposits that accounted for 7–13% of glomerular area (Figure 4A-D). Immunostaining analysis further confirmed that in comparison to Myo1c$^{fl/fl}$pod-Cre$^{Tg/+}$ mice, the expression of α-SMA was significantly increased in Myo1c$^{fl/fl}$ mice upon injury (Figure 4E-F).

In a similar fashion, fibrosis was also evaluated in NTS injury model, where kidney sections were analyzed at day 6 post NTS injection. Sirius-red staining showed a significant increase in glomerular fibrotic areas (~6%) in Myo1c$^{fl/fl}$ mice, when compared to the Myo1c$^{fl/fl}$pod-Cre$^{Tg/+}$ mice (~2%) (Figure S5C-D). Accordingly, in comparison to Myo1c$^{fl/fl}$pod-Cre$^{Tg/+}$ mice, increased α-SMA staining was noted in the Myo1c$^{fl/fl}$ mice (Figure S5E-F). Collectively, these results show that podocyte-specific deletion of Myo1c attenuates injury-induced fibrosis in mice glomeruli.

## Renal fibrosis is attenuated in podocyte-specific Myo1c knockout mice following unilateral ureteral obstruction (UUO).

Since TGF-β is the master regulator of fibrosis and glomerular fibrosis was attenuated in these models, it prompted us to test whether the loss of Myo1c affects TGF-β dependent renal fibrosis in mice.[39,40] Therefore, mice were subjected to UUO procedure, which is an established model of TGF-β dependent renal fibrosis[39,41] (Figure 5A). The histological analysis of obstructed kidney showed characteristic enlargement of renal pelvis and thinning of renal cortex[41,42] (Figure 5B); in addition, increased loss of renal pelvis area was noted in the control mice sections compared to Myo1c$^{fl/fl}$-podCre$^{Tg/+}$ mice (Figure 5B). Total renal

area analysis (normalized with sham) further revealed that Myo1c$^{fl/fl}$-podCre$^{Tg/+}$ mice lost ~20% renal area, whereas the control Myo1c$^{fl/fl}$ mice lost ~30% renal area at 7 days post UUO procedure (Figure 5D). It was also noted that in comparison to the control mice, distinct renal layers, cortex and lower medulla were well preserved in Myo1c$^{fl/fl}$-podCre$^{Tg/+-}$ mice (Figure 5B). Additionally, the Myo1c$^{fl/fl}$ mice sections showed more fibrotic lesions and increased tubular dilation (Figure 5B). The Sirius-red and masson's trichrome staining of renal sections further showed increased interstitial fibrosis in Myo1c$^{fl/fl}$ mice kidney, when compared to Myo1c$^{fl/fl}$-podCre$^{Tg/+}$ mice kidneys (Figure 5E). Immunostaining of kidney sections showed increased α-SMA expression in the glomeruli of control mice; in contrast, the staining of α-SMA in Myo1c$^{fl/fl}$-podCre$^{Tg/+}$ mice sections was comparable to sham mice (Figure 5F-G). Notably, this is the most intriguing part of this study that a podocyte-specific knockout has a global effect in kidney and further supports the value of cross talk between various renal cells. Collectively, these results are in agreement with other injury models tested in this study, supporting a profibrotic role for Myo1c.

### TGF-β-induced signaling is attenuated in Myo1c knockdown (Myo1c-KD) podocytes:

Since TGF-β signaling is the primary driver of glomerular and renal fibrosis,[6,43,44] we hypothesized that podocyte-specific loss of Myo1c affects TGF-β signaling to mediate this phenotype. To test this, the activation profiles of key TGF-β signaling components in Myo1c-KD podocytes were investigated. Results showed significant reduction in canonical and non-canonical pathway components including phospho-SMAD3, phospho-p38 and phospho-ERK2/3 (Figure 6A-B). Notably, the fibrotic marker α-SMA, was also attenuated in TGF-β treated Myo1c-KD podocytes, which was also confirmed by a significant reduction of α-SMA immunostaining in Myo1c-KD podocytes (Figure S6). Further comparative analysis of TGF-β stimulated Myo1c-KD (Figure 6A) and Myo1c overexpressed podocytes (Figure 6C) showed that while Myo1c-KD blunted TGF-β signaling, the overexpression of Myo1c, increased the expression of various TGF-β signaling components including phospho-SMAD2/3 and phospho-ERK2/3 (Figure 6C-E). Collectively, these results provide evidence for anti- fibrogenic response in Myo1c depleted podocytes.

### Myo1c-KD in cultured human podocytes blunted TGF-β induced expression of multiple genes and cellular events.

Since podocyte-specific Myo1c knockout mice showed reduced renal fibrosis, we hypothesized that loss of Myo1c may blunt TGF-β- induced cellular response. To test this hypothesis, Myo1c-KD podocytes were stimulated with TGF-β/vehicle and subjected to mRNA profiling. Principal component analysis (PCA) showed that biological replicates within each group were most similar to each other and segregated from the experimental groups (Figure S7A). RNA-seq data was submitted to Gene Expression Omnibus (GEO) data base (# GSE118816). The heat map from RNA-Seq data showed DE genes in the control and Myo1c-KD with and without TGF-β stimulation (Figure 7A). The volcano plots showed that TGF-β treatment resulted in a significant increase in number of DE genes in both control and Myo1c-KD podocytes (Figure S7B-D). Further, gene ontology (GO) enrichment analysis was performed, which identified several major biological processes ($p<0.05$) including endocytosis, actin cytoskeleton organization, kidney development, cell

cycle progression, and transcription (Figure 7B). Since loss of Myo1c affected all these cellular processes that are also involved in progression of TGF-β induced renal fibrosis,[45,46] it is likely that this contributes to the attenuation of injury phenotype observed in Myo1c$^{fl/fl}$-podCre$^{+/-}$ mice. Interestingly, highest enrichment was observed in the pathways involved in transcriptional regulation through RNA polymerase II promoter and Negative regulation of transcription (Figure 7B). These results further indicated participation of Myo1c in transcriptional regulatory events in podocytes, which is in agreement with the recently described role for the nuclear isoforms of Myo1c.[20,22] This led us to hypothesize that TGF-β may affect the expression of nuclear myosins in these cells. Thus, the expression of various Myo1c isoforms was evaluated using qPCR following TGF-β treatment of cultured human podocytes (which contains both NM1 isoforms). Interestingly, treatment with TGF-β significantly upregulated the gene expression of Myo1c in a time dependent fashion, which was attributed to specific increase in the nuclear Myo1c isoforms NM1(N16) and NM1(N35) (Figure 7C). To further confirm, if injury also induces a similar increase in the nuclear myosin, glomeruli from mice treated with ADR were evaluated for the expression of Myo1c using qPCR analysis. Similar to the TGF-β treatment, ADR also selectively induced NM1(N16) expression level (Figure 7D). Lastly, to confirm if Myo1c-KD resulted in specific depletion of all Myo1c isoforms including NM1(N16) and NM1(N35), we evaluated the expression of these Myo1c isoforms using qPCR (Figure 7E). The results showed that expression of all Myo1c isoforms was significantly attenuated in human podocytes (Figure 7E). To further evaluate if loss of Myo1c had an effect on genes associated with slit-diaphragm and podocyte injury or apoptosis, heatmap of control and Myo1c-KD podocytes treated with TGF was generated. Analysis from these cells further showed that the loss of Myo1c reversed or neutralized the gene expression signature of TGF-β treatment (Figures S7E&F). Collectively, these results led us to hypothesize that NM1 actively participates in podocyte injury and are suggestive of a mechanism through which, loss of these nuclear myosins in our transgenic models may attenuate transcription of target genes that are critical for injury progression, thus resulting in a protective phenotype.

### NM1 targets TGF-β responsive genes to regulate TGF-β signaling.

To further decipher the mechanism through which NM1 regulates TGF-β signaling, we investigated if NM1 is involved in transcriptional regulation of TGF-β responsive genes. A recent study, where Chip-Seq analysis of NM1 was performed in mouse embryonic fibroblasts showed that Myo1c associated with various gene promoters[47], which supported a transcriptional role for NM1[47,48]. To identify which of these genes were DE in response to TGF-β stimulation, we performed a comparative analysis, where our mRNA profiling data was compared with the data presented in their analysis (Supplemental data in Almuzzaini B et al.[47]). This led to the identification of 45 genes, that were DE in response to TGF-β stimulation among which, 9 genes showed upregulation (Figure 8A). To determine which of these genes are targeted by NM1, we evaluated changes in their gene expression in TGF-β treated Myo1c-KD podocytes. Interestingly, only GDF-15 and JunB genes were upregulated in response to TGF-β and loss of Myo1c downregulated their expression (Figure 8B), indicating these as NM1 targets. Notably, in comparison to the JunB gene, significant downregulation of GDF-15 gene was observed (Figure 8B). To further confirm these observations, we evaluated the expression of GDF-15 and JunB proteins in Myo1c-KD cells.

Similar to the qPCR results, loss of Myo1c blunted TGF-β-induced upregulation of GDF-15, whereas minimal downregulation of JunB was noted (Figure 8C-D). To further support that GDF15 and JunB are involved in podocyte pathogenesis, we investigated the expression of these genes using qPCR analysis of cultured podocytes treated with PS and NTS. The results showed that GDF-15 and JunB, were consistently upregulated in both the injury models tested (Figure 8E). To further determine the involvement of these genes in podocyte disease pathogenesis, we performed immunofluorescence staining analysis of kidney sections from the FSGS patients (Table S4). The results showed that GDF-15 was significantly upregulated in the glomeruli of FSGS patients (Figure 8F & Figure S8A&B). In contrast no upregulation was noted for JunB protein, indicating that GDF-15 may be the primary gene involved in disease pathogenesis of podocytes (Figure S8A-C). To further confirm the involvement of GDF15 in disease pathogenesis, we evaluated the expression of GDF15 in the glomeruli of mice injured with ADR or NTS. Similar to FSGS patients, we saw a significant increase of GDF15 in the glomeruli of injured mice (Figure S9A-E). To further confirm NM1 dependent GDF15 increase, a rescue experiment was performed, where the Myo1c-KD human podocytes were rescued by over-expressing mouse GFP-Myo1c. While we did not see any upregulation of GDF15 in TGF-β treated Myo1c-KD cells, there was a significant upregulation of GDF15 when GFP-Myo1c was overexpressed in these podocytes (Figure S9F-G). To further confirm these observations another rescue experiment was performed, where NM1 was overexpressed in Myo1c-KD podocytes. Expectedly, the NM1 over-expression significantly upregulate the GDF-15 expression in response to TGF-β treatment (Figure S10A-C). In conclusion, the overall results support a mechanism, where injury induces the upregulation of NM1, which transcriptionally regulates TGF-β responsive gene GDF-15 and hence, podocytes response to injury.

### GDF-15 is the transcriptional target of NM1.

Since GDF15 was selectively upregulated in human FSGS patients, we next wanted to determine if NM1 transcriptionally targets GDF15. Therefore, we first investigated the binding between NM1 and GDF15 promoter by ChIP-qPCR using various primer sets representing the GDF15 promoter region (schematic Fig 8G). The ChIP analysis from human podocytes showed significant enrichment in the binding between Myo1c and GDF-15 promoter, when compared to the control IgG antibody (Figure 8G). Interestingly, the NM1 binding was enriched at the transcriptional initiation site (GDF-15 primer, F1/R1). This enrichment was further confirmed by gel electrophoresis, which showed increased GDF15 promoter binding to NM1 (Figure S10D). These results are consistent with the binding of P53 to GDF15 promoter, which is known to affect the transcription of GDF15[49]. Next, we performed DNA-protein interaction to evaluate a direct interaction between Myo1c and GDF promoter. Therefore, purified Flag-Myo1c protein was immobilized on Flag agarose beads and incubated with the PCR amplified and purified GDF15 promoter region. The bound promoter was evaluated by qPCR and the results showed more than three folds enrichment in the binding of GDF15 promoter to Myo1c when compared to the control, where no Myo1c protein was added (Figure S10E). These findings further confirm GDF-15 as a transcriptional target for Myo1c.

### GDF-15 contributes to podocyte susceptibility to injury:

Since GDF15 is involved in disease pathogenesis,[50,51] and our results further support this concept, we hypothesized that increased expression of GDF15 may enhance podocytes susceptibility to injury. Thus, injury-induced apoptosis using protamine sulphate[52] was measured in human podocytes over-expressing GDF-15. The FACS analysis showed significantly increased apoptotic cells (63.1%) in GDF15 overexpressing cells, when compared to the control cells (43%) (Figure S11). These results are in agreement with data from Myo1c-KD podocytes, where loss of Myo1c attenuated GDF15 expression and protected them from injury.

## DISCUSSION

Podocyte injury is central to many glomerular diseases,[3,5,30] yet the molecular mechanisms that are involved in injury progression are poorly understood. While TGF-β signaling has been shown to play a critical role in podocyte injury,[6,7] its regulation in podocytes remain unclear. In this study, we show a novel role for the motor protein Myo1c in disease pathogenesis, where Myo1c regulates TGF-β signaling to generate an injury response from podocytes. Specifically, we describe the construction and characterization of a tissue-specific Myo1c knockout mouse model, and show that podocyte-specific knockout of Myo1c prevents progression of glomerular injury in mice. These results are in direct contrast with our previously published systemic Myo1c-KD study in zebrafish,[53] where morpholino mediated systemic knockdown induced a glomerular phenotype. Since Myo1c is widely expressed and involved in multiple cellular and nuclear events,[13,53] a systemic loss of Myo1c may induce a cumulative phenotype that may result in severe functional defects leading to organ damage. Importantly, these previous studies may provide little information about a cell-specific role for this protein. The present study reaffirms the significance of tissue specific genetic deletion models for proteins that may reveal their novel cell-specific roles and thereby define key events in a cell where the target protein participates.

The development of Myo1c floxed mice, provided us with a unique opportunity to study the cell-specific function of Myo1c. Contrary to our expectations, genetic deletion of Myo1c in podocytes did not result in any renal insufficiency or proteinuria even when mice were aged to ~12 months. This prompted us to test a second hit hypothesis, where we tested the susceptibility of $Myo1c^{fl/fl}$-$podCre^{Tg/+}$ mice to various glomerular injury inducing agents including adriamycin and NTS.[26,27,38] Most notably, the injuries by these agents are characterized by podocyte actin cytoskeletal reorganization leading to its effacement.[27,35,36] Interestingly, unlike the control, $Myo1c^{fl/fl}$-$podCre^{Tg/+}$ mice were protected from adriamycin and NTS induced injuries. This protection was apparent at both, the physiological and structural levels (Figure 2&3). Although it is likely that injury is induced in these models via separate mechanisms, these mechanisms are either regulated through a common regulatory event/s or they converge onto a common pathway and Myo1c may participate in those events thereby regulating podocytes response to injury. Notably, these results are in sharp contrast with the podocyte- specific deletion of Myo1e,[54, 55] but are consistent with loss of proteins in podocytes that are involved in podocyte signaling such as Rac1 and Crk.[36,56,57] Interestingly, podocyte-specific deletion of Glut4, a glucose

transporter and Myo1c binding protein was also shown to protect podocytes from diabetic nephropathy,[58] suggesting that Myo1c may participate in mechanisms that are involved in podocytes response to injury.

Fibrotic changes mainly glomerulosclerosis and tubulointerstitial fibrosis are visualized in many glomerular diseases and animal models of podocytes injury including adriamycin and NTS.[28,29,35] The attenuation of injury-induced fibrosis in the Myo1c$^{fl/fl}$pod-Cre$^{Tg/+}$ mice provided primary evidence that loss of Myo1c in podocytes may affect fibrotic signaling pathway. The profibrotic role of Myo1c was further demonstrated using the UUO interstitial fibrosis model (Figure 5), where podocyte specific Myo1c deletion attenuated kidney fibrosis. It was interesting to note that while Myo1c was specifically deleted in podocytes, it affected the development of fibrosis in entire kidney. This suggests that podocytes may play a central role in the progression of kidney fibrosis; however, this concept needs to be further investigated. Since increasing evidences now suggest that podocytes in conjunction with endothelial cells and glomerular basement membrane (GBM) form the glomerular filtration assembly[59], it is likely that functional changes to podocytes may positively or negatively influence the functioning of these cells and vice-versa. Moreover, recent evidences have shown intercellular crosstalk between various glomerular cell types and segments of kidney[60,61], because of which, the effect on one cell type may be propagated to others leading to a diseased phenotype.

Since TGF-β1 is the master regulator of renal fibrosis in multiple cell types including podocytes,[37,44] where it regulates a variety of cellular functions through a multitude of intracellular signaling pathways, blunting of TGF-β1 signaling by Myo1c may attenuate the injury response of podocytes. This was also supported from our cell culture studies, where, α-SMA, a marker for fibrosis was remarkably reduced in TGF-β stimulated Myo1c-KD podocytes (Figure S6). TGF-β is rapidly becoming an attractive therapeutic target in treatment of various diseases including cancer, systemic sclerosis and cystic fibrosis.[62,63,64] Involvement of TGF-β signaling as a key player in podocyte fibrosis was shown in a recent study where a TGF-β neutralizing anti-TGF-β antibody, 1D11 prevented glomerular fibrosis and protected podocytes from injury and preserved renal function.[65] Interestingly, we also find that loss of Myo1c in podocytes attenuated injury- induced fibrosis in our *in-vivo* models and preserved podocyte morphology and function. However, the evidence for involvement of Myo1c in TGF-β signaling came from our cell culture and qPCR analysis, which showed that loss of Myo1c in podocytes specifically blunted both TGF-β canonical and non-canonical pathway signaling. Collectively, these results suggest that Myo1c may be involved in development of injury-induced fibrosis through TGF-β signaling.

Based on the published literature, Myo1c may be involved in several cellular events that define cell survival and function.[11,14,16,66] Indeed, comparative analysis of TGF-β induced control and Myo1c-KD podocytes suggested that Myo1c participates in a variety of cellular events that define podocyte survival and function (Figure 7B). Strikingly the cellular events that are involved in transcriptional regulation were highly enriched indicating a novel nuclear specific role for Myo1c in podocytes. This is in agreement with the proposed function of nuclear form of Myo1c (NM1), which was shown to interact with RNA polymerases and involved in transcription.[20,22] The significance of NM1 was further

implicated from the qPCR analysis, where injury to podocytes significantly upregulated the expression of nuclear myosins (Figure 7D) further suggesting that nuclear myosins actively participate in the progression of injury. This further implies that the downregulation of TGF-β signaling may be mediated by NM1 at the transcription level, thereby regulating podocytes response to injury. While the data indicated critical role for NM1, the contribution from cytoplasmic Myo1c isoform cannot be ruled out, especially since other cellular events such as vesicular transport were also affected, albeit at a much lower level (Figure 7B). The significance of these observations needs to be further investigated in detail.

The identification of TGF-β responsive genes GDF-15 and JunB as Myo1c targets provides novel molecular insight into the regulation of TGF-β signaling by Myo1c. Both GDF-15 and JunB are activated in response to TGF-β and are involved in disease pathogenesis,[44,50,67,68] and therefore, attenuation of these genes will have profound effect on the podocytes ability to respond to injury. Indeed, these genes were downregulated in Myo1c-KD podocytes suggesting that their downregulation may contribute to the protective phenotype observed in our podocyte-specific Myo1c knockout mouse models. While GDF-15 is the member of TGF-β superfamily, JunB is a member of the activator protein-1 family of dimeric transcription factors and importantly, both were found to associate with NM1. GDF-15 is known to be involved in the pathogenesis of systemic sclerosis, pulmonary fibrosis and cancer development, progression and metastasis.[50,68,69] We find that GDF-15 expression was elevated in response to NTS and PS, which is consistent with other reports, where increased plasma levels of GDF-15 has been noted in inflammation, acute injury and cancer.[50,67,69] GDF15 is also known to participate in fibrosis through its ability to associate with matrix metalloproteinases and sST2 (soluble suppression of tumorigenicity-2) proteins that are molecular targets of fibrosis.[70] The other target JunB has been shown to mediate promoter activity of COL1A2 gene, which encodes for collagen type I protein, the main component of extracellular matrix involved in fibroblast differentiation leading to scarring and fibrosis.[68] Overall, the results from this study suggest that while both TGF- β responsive genes GDF-15 and JunB were targeted by Myo1c, the expression of GDF- 15 was most affected by the loss of Myo1c. Moreover, GDF-15 was highly upregulated in human FSGS patient samples, further indicating that GDF-15 may play a critical role in the pathogenesis of podocytopathy. Importantly, the, ChIP and DNA-protein binding analysis showed significant enrichment of NM1 binding at the GDF-15 promoter (Figure 8G) suggesting that NM1 may directly regulate the transcription of GDF-15 gene. Collectively, these results support a transcriptional regulatory role for Myo1c, where Myo1c mediated regulation of TGF-β responsive genes is central to disease progression in podocytes (Figure 9).

## METHODS

### Generation of Myo1c flox/flox mice:

Myo1c$^{fl/fl}$ mice were generated using embryonic stem (ES) cells containing the Myo1c targeting vector as depicted in figure 1. ES cells were obtained from the European Conditional Mouse Mutagenesis Program (EUCOMM) and were implanted in foster mother at the Transgenic Chimeric Mouse Facility of the University of Pennsylvania. Since these ES cells were derived from C57BL/6N genetic background, they were microinjected in the same

genetic background mice to generate chimeras. Although EUCOMM validated the targeting construct using long range PCR, we employed various strategies to further validate the construct and its germline transmission including 5' and 3' arm long range PCR and DNA sequencing as shown in figure S1. List of the primers used for the validation through the long range PCR is provided in table S1. Validation of 5' homology arm was performed using the primer sets GF1, GF2, GF3 or GF4 and LAR3, which generated around 6kb PCR product (Figure S1B-C). Validation of the 3' homology arm was performed using primer sets RAF5 and GR1, GR2, GR3 or GR4, which generated a PCR product of ~11 kb (Figure S1C-D). Further validation of the targeting vector was performed using additional primer set FP1 and GR4, which generated a ~6kb PCR product (Figure S1B&1D). The PCR products described above (representing the 3' and 5' arms) were gel purified and sequenced to further validate the correct orientation and insertion in the targeting vector. To test whether the Myo1c floxed gene can be excised by Cre enzyme, *in vitro* validation was performed by incubating the DNA isolated from ES cells with Cre enzyme followed by PCR using RAF5 and 2RP primers. As shown in figure S1E&F, the expected excision of LoxP sites generated two distinct bands of 200–300bp from the targeting vector confirming the fidelity of LoxP sites. It is to be noted that wild-type gene (that does not contain flox sites) could not be digested by the cre enzyme and it generated a PCR product of ~6kb that was not amplified in this reaction. Chimeric mice obtained from the foster mother were further bred to generate more pups and were backcrossed with the flp mice to remove the neo cassettes. Removal of neo cassette was confirmed through PCR. All neo negative mice were backcrossed seven or more generations with C57BL/6N, C57BL/6J and FVB mice strains to generate pure line of $Myo1c^{fl/fl}$ mice on these genetic backgrounds.[71] The floxed mice were crossed with podocin cre (B6.Cg-Tg(NPHS2-cre)295Lbh/J) mice to remove Myo1c protein specifically in podocytes. This strategy targeted the deletion of critical Myo1c motor domain (exons 6–14) resulting in a frame shift mutation that causes premature termination in Myo1c open reading frame. Hence, this targeting strategy resulted in deletion of all reported Myo1c isoforms (Figure 1A). The podocyte-specific Myo1c knockout mice ($Myo1c^{fl/fl}$pod-$Cre^{Tg/+}$), and their littermate controls ($Myo1c^{fl/fl}$, $Myo1c^{fl/+}$pod-$Cre^{Tg/+}$ and $Myo1c^{+/+}$pod-$Cre^{Tg/+}$), were born without any developmental defects with normal Mendelian frequency (data not shown). Two different primer sets (Table S2) were used to genotype the homozygous ($Myo1c^{fl/fl}$), heterozygous ($Myo1c^{fl/+}$) and wild-type ($Myo1c^{+/+}$) mice. These mice were further crossed with Gt(ROSA)26Sortm4(ACTB-tdTomato,-EGFP)Luo/J (Jackson laboratory # 007576) mice to specifically induce the expression of GFP in podocytes. The GFP expressing podocytes were isolated by FACS sorting through established procedure as discussed previously and used for further analyses[25].

## Primary Kidney Cells:

Primary kidney cells were isolated from $Myo1c^{fl/fl}$ mice using a conventional method.[72] Briefly, Kidneys were isolated from mice and minced using sterile blade. Dissociation of cells was performed by incubating them in 0.25% trypsin for 15–20 minutes at 37°C. Primary cells were plated (10$cm^2$ plates) and treated with either Adeno-Cre virus or β-Gal virus for a period of 24 hours. After 24 hours the cells were washed and replaced with normal DMEM medium containing 10% FBS and 1% penicillin and streptomycin and incubated for additional 96 hours. Cells were lysed in RIPA buffer and western blotting was

performed using anti Myo1c, Myo1b and actin antibodies to investigate the efficacy of cre excision in Myo1c$^{fl/fl}$ primary kidney cells.

### Isolation of mice glomeruli:

Mice glomeruli were isolated using the magnetic beads- based method as described previously.[26,33] Total RNA was isolated and Myo1c expression in Myo1c$^{fl/fl}$ and Myo1c$^{fl/fl}$podCre$^{Tg/+}$ mice glomeruli was evaluated by qPCR using specific primers. Details of mouse Myo1c and NM1 primers used for qPCR are provided in Table S2.

### Podocytes Injury model:

All experiments were performed in 8–12 weeks old mice and littermates were used as controls. 15mg/kg adriamycin (doxorubicin hydrochloride) was injected retro-orbitally into C57BL/6N background mice as described previously.[18,28] Pre-injection and post-injection urine samples were collected from individual mice on a weekly basis for 4–5 weeks. Nephrotoxic serum (NTS) was used to induce acute glomerular injury in mice. 100μl of NTS was injected retro-orbitally as described previously.[35,36] Pre-injection and post-injection urine samples were collected from individual mice as indicated. Any urine sample that was contaminated with mice feces was discarded. Urine samples were spun down at 4000xg for 5 minutes and then frozen at −80°C for future experiments. All urine samples were run on 10% SDS-PAGE and examined by Coomassie blue staining. Urine albumin/creatinine ratios were obtained using an enzyme-linked immunosorbent assay (ELISA) Albuwell kit (Exocell) and creatinine companion kit (Exocell), and the results were analyzed either by 2-way ANOVA (Sidak's multiple comparison test) or 1-way ANOVA (Kruskal-Wallis test) (GraphPad Prism 7).

### Sample preparation, Immunohistochemistry and Electron Microscopy:

Mice were anesthetized with Avertin (2, 2, 2-Tribromoethanol) prior to the procedure. Mice kidneys were perfused with Hanks buffered salt solution (HBSS) for 5 min followed by 4% paraformaldehyde in HBSS for 15 min at 80 to 100 mm Hg, retrograde to the intrarenal aorta of anesthetized mice using a 24-gauge angiocatheter (BD Biosciences). Perfused kidneys were decapsulated, washed with 1X PBS, transected, fixed for 4 to 12 h in 4% paraformaldehyde, rinsed, and sequential alcohol treatments were performed and submitted to the Abramson Histology Core (University of Pennsylvania) or Medical University of South Carolina (MUSC), Histology Core facility. The paraffin embedded sections were deparaffinized and stained with Masson's trichome and Sirius Red for histological analysis. Staining of various proteins including Neph1, Nephrin, ZO1, synaptopodin, Myo1c, phospho-Neph1 and phospho-Nephrin was performed using specific antibodies as described previously.[18,36] A Zeiss inverted microscope (Zeiss Axio Observer D1m) fitted with 63X and 25X oil immersion objectives was used for fluorescence microscopy, The confocal Microscopy was performed at the Molecular Pathology & Imaging Core (MPIC) of the University of Pennsylvania or the molecular and imaging core of the MUSC. The acquisition of microscopic images was performed using Metamorph software. All parameters were maintained constant throughout the image acquisition, including the exposure time. The image J software was used for quantitative analysis. Multiple images from 3 or more mice were used for each quantitative analysis. Representative images from three or more

independent experiment were used to generate each figure. For scanning and transmission electron microscopic (SEM and TEM) analysis, the Kidney samples were kept in a mixture of 2% glutaraldehyde and 2% paraformaldehyde solution overnight for fixation. Samples were processed, sectioned and imaged at the Biomedical Imaging Core/Electron Microscopy Resource Laboratory of the University of Pennsylvania and the Department of pathology, MUSC. Five to ten glomeruli per sample from a minimum of three mice were evaluated and slit diaphragm frequency was quantitatively assessed by counting the number of junctions per micron of basement membrane using Image J software.

### Cell Culture and TGFβ stimulation:

The human podocyte cell line was cultured in RPMI 1640-based medium supplemented with 10% fetal bovine serum (FBS) (Invitrogen), 2 g/liter of sodium bicarbonate ($NaHCO_3$), insulin-transferrin-selenium (ITS) supplement (Sigma-Aldrich), and 200 units/ml penicillin and streptomycin (Roche Applied Science) as described previously.[32,73] The podocyte cells were grown on collagen-coated culture dishes at 33°C and 5% $CO_2$, and were differentiated by thermo switching to 37°C as described previously.[32,73] Myo1c-KD in human podocytes was performed using specific lentiviral shRNA particles obtained from sigma (SHCLNV-NM_033375; TRCN0000122927) as described previously.[18] In a similar fashion Myo1c in mouse podocytes was knocked down using specific shRNA lentiviral particles obtained from sigma (SHCLNV-NM_008659; TRCN0000100744). Scramble ShRNA were also obtained from sigma and used as controls. Rescue experiment was performed in Myo1c-KD human podocytes by over-expressing mouse GFP-Myo1c. Viral constructs encoding GFP-Myo1c, NM1 and GDF-15 were prepared by standard cloning in the pBABE vector[18]. Differentiated human podocytes were stimulated with TGF-β as described.[32] Briefly, podocytes were incubated overnight in RPMI medium with 0.1% FBS and stimulated with 5ng/ml of TGF-β in the same medium for a period of 48hours. Control and TGF-β stimulated podocytes were processed for protein and RNA analysis using standard protein lysis and RNA isolation kits respectively. All the experiments were performed in triplicates.

### RNA-Seq and bioinformatics analysis:

RNA samples isolated from the human podocytes were submitted to the Novogene Genome Sequencing Company, which performed the quantitative and qualitative assessment of RNA samples including the RNA integrity and contamination. The library construction was performed by the company using poly-T oligo-attached magnetic beads. The libraries were fed into HiSeq/MiSeq illumina machines for RNA sequencing. Bioinformatics downstream analysis was performed by Novogene Genome Sequencing and the bioinformatics core of the MUSC using a combination of programs including Bowtie2, Tophat2, HTseq, Cufflink and our wrapped scripts. Briefly, reference genome and gene model annotation files were obtained from NCBI/UCSC/Ensembl genome browser. Indexes of the reference genome were built using Bowtie v2.0.6 and paired-end clean reads were aligned to the reference genome using TopHat v2.0.9. Quantification of gene expression level was analyzed using HTSeq v0.6.1 and read numbers counts were mapped for each gene. Reads Per Kilobase of exon model (RPKM) for each gene was calculated based on the length of a gene (Mortazavi et al., 2008). Differential expression analysis was performed using the DESeq2 R package (2_1.6.3). DESeq2 provides statistical routines for determining differential expression in

digital gene expression data using a model based on the negative binomial distribution. The resulting P-values were adjusted using Benjamini and Hochberg's approach and adjusted P-value <0.05 reported by DESeq2 were assigned as DE. DEGSeq R package (1.12.0) was used to analyze differential expression under TGF-β stimulated and unstimulated conditions. The P values were adjusted using the Benjamini & Hochberg method. Corrected P- value of 0.005 and log2(Fold change) of 1 were set as threshold to classify as significant differential expression. Correlations were determined using the cor.test function in R with option set alternative - 'greater" and method = "Spearman". To identify the correlation between difference, we clustered different samples using expression level RPKM to visualize correlation using hierarchical clustering distance method with the heatmap function, SOM (Self-organization mapping) and kmeans using silhouette coefficient to adapt the optimal classification with default parameter in R. Gene ontology (GO) and KEGG enrichment analysis of DE genes was performed using the GOseq R package. KOBAS software was used to test the statistical enrichment of differential expression genes in KEGG pathways. RNA-seq data was submitted to Gene Expression Omnibus (GEO) data base (https://www.ncbi.nlm.nih.gov/geo/querv/acc.cgi9acc-GSE118816).

### Western blotting, antibodies and reagents:

Primary kidney cells and human podocytes were lysed in RIPA buffer and protein estimation was performed using the BCA method. 20μg protein samples from lysates were used for western blotting analysis. Myo1c, Neph1, Nephrin and Myo1b antibodies have been described previously.[18,31,32] Other antibodies, including GAPDH (Sigma # G8795), α-SMA (Santa Cruz # c-53142), NM1 (Sigma # M3567), phospho-SMAD2 (Invitrogen # 44–244G), phspho-SMAD3 (Millipore # 07–1389), SMAD2/3 (Cell Signaling # 3102S), phospho-p38 (Santa Cruz # sc-166182), p38 MAPK (Cell Signaling # 9212S), phospho-JNK (Cell Signaling # 9255S), JNK (Cell Signaling # 9252S), phospho-ERK1/2 (Cell Signaling # 9101), ERK1/2 (Cell Signaling # 4695S), GDF-15 Antibody (Santa Cruz # sc-377195) and JunB Antibody (Santa Cruz # sc-8051) were commercially obtained. Western blotting image acquisition and densitometric analysis was performed using LI-CORE imaging station. The fluorophore secondary antibodies, Alexa Fluor 488 goat anti-rabbit IgG (H+L), Alexa Fluor 568 goat anti-mouse IgG (H+L) and Alexa Fluor phalloidin were commercially obtained from Invitrogen. Doxorubicin hydrochloride (adriamycin) was purchased from R&D Systems, Inc. Nephrotoxic serum was obtained from Dr. David Salant[74] and Probetex Inc. (PTX-001) and used as previously described.[26,36]

### Unilateral Ureter Obstruction (UUO) animal model:

Myo1 cfl/fl and Myo1cfl/flpod- $CreTg^{/+}$ mice (12–14weeks, n= 6, each) were subjected for UUO procedure as described.[39,42] Briefly, Male and female mice were weighed and treated with buprenorphine (0.09 – 0.1 mg/kg, sc). Mice were anesthetized (Isoflurane: 5% induction, 2% maintenance) and placed on a thermo-regulated heating pad at 37°C. The lower pole of left kidney was exposed via an upper flank incision, and the ureter was tied off with at least 2 sutures (5–0 Ethilon) - in line with the lower pole and several mm distal to the first tie. Sham-operated animals underwent same surgery without the obstruction of ureter. All mice were treated with buprenorphine (0.09–0.1 mg/kg, sc, q11–13 hours until completely recovered). Seven days post procedure, all mice were sacrificed and contralateral

and obstructed (injured) kidneys were harvested. Kidneys were saggitally cut and half of each kidney was fixed in 4% PFA for histological analysis, whereas the other half was cryo-freezed for protein analysis. Parafilm embedding, sectioning, Masson's trichrome and Sirius stainings were performed at the MUSC histology core. Masson's trichrome stained kidney slides were scanned at various magnifications (4x, 20x and 40x) using Olympus BX61 Microscope (Olympus BX61 Microscope) at Laboratory Core in the Center for Oral Health Research. Slides were also Immunostained with α-SMA and Nephl antibodies and mounted with DAPI. The confocal images were collected on Olympus FV10i laser scanning confocal microscope and processed images were used to measure mean fluorescence intensity using Image- J software. The fibrotic areas were manually outlined and analyzed using image-J software.

### Expression analysis:

Total RNA isolation was performed from differentiated human podocytes treated with 5% NTS or protamine sulphate (500μg/ml) for 8hours. Untreated differentiated podocytes were used as a control. Details of the primers used for qPCR are presented in Table S2.

### ChIP-qPCR analysis:

Chromatic immunoprecipitation was performed using the EpiTect ChIP One-Day (Qiagen) as per the manufacturer instructions. Briefly, differentiated human podocytes were cross-linked and fixed using fresh fixing buffer, washed and chromatin shearing was performed using cell harvesting buffer. Sheared chromatin was diluted and re-suspended in IP lysis buffer, which was pre-cleared using protein A beads before proceeding to chromatin immunoprecipitation. About 3μg of Nuclear Myo1c, NM1 antibody or Control IgG rabbit antibody was added to the DNA-bound protein mixture and immunoprecipitation was performed using protein A beads. IP fraction was washed with washing buffer I-IV as per manufacture's protocol. Following IP, the crosslinks were reversed, protein was removed and DNA purification and isolation was performed using extraction beads and DNA spin column and finally chipDNA was eluted using the elution buffer. qPCR was performed using GDF-15 primers from the promoter region from the input sample and equal amounts of NM1 (Sigma) and IgG-rabbit (Thermo fisher) antibody immunoprecipitated ChIP-DNA samples (Table S3). Three different sets of GDF-15 primers as shown in the schematic figure 9A were used to define the enrichment region for binding. The enrichment of GDF15 was analyzed using relative fold changes through qPCR and agarose gel electrophoresis.

### DNA-Protein Binding Assay:

The DNA protein binding assay was performed as described with slight modifications[75]. Briefly, purified Flag-Myo1c protein (0.2μM) was added to flag agarose beads[76]. The beads were washed with PBS and incubated with 20 fmol of PCR amplified and purified GDF15 promoter (using the primers 1F/R) in the presence of binding buffer (10 mM Tris pH 7.5, 100 mM NaCl, 1 mM dithiothreitol, 5 mM EDTA, 4% (v/v) glycerol and 0.08 mg/ml sonicated salmon sperm DNA) at room temperature for 20 minutes. The prewashed Flag-agarose beads without Flag-Myo1c protein were used as a negative control. Next, beads were washed twice with PBS, twice with wash buffer (10 mM Tris-HCl [pH 8.0], 0.25 M LiCl, 0.5% NP-40, 0.5% sodium deoxycholate, and 1 mM EDTA), and twice with TE (10

mM Tris-HCl [pH 7.5], and 1 mM EDTA [pH 8.0]) at RT. DNA was eluted by incubating the beads with 200 μl of elution buffer (50 mM TrisHCl [pH 7.5], 10 mM EDTA [pH 8.0], and 1% SDS) at 65Ό for 15 min. The supernatant containing eluted DNA-protein complex was collected, 20 μg proteinase K was added to digest the DNA bound peptide and incubated further at 42°C for 2h. The DNA was column purified using Qiagen PCR purification kit, and subjected to quantitative real-time PCR analysis using SYBR green Supermix (Cat no: 172–5270; Bio-Rad, CA) according to the manufacturer's instructions. The q-PCR primers (GDF15- N1F/R) from GDF15 promoter region are described in Figure 8G. Quantification was performed using the CT method. Briefly, threshold cycle (CT) values obtained by the binding reactions with flag Myo1c protein were normalized by the control (without Myo1c) and followed by linear conversion of dCT values (Ref 2). Error bars represent standard error.

### Measurement of cellular apoptosis in GDF-15 over-expressed cultured human podocytes:

The cultured human podocytes stably expressing Flag-GDF-15 protein were constructed using virally transduced Flag-GDF-15 construct and puromycin selection as described earlier[18]. The control and GDF-15 over-expressing cultured podocytes were treated with protamine sulphate as described previously[77]. Following over-night treatment, the cells were trypsinized and incubated with FITC-annexin V and propidium iodide for 15 min in annexin V binding buffer as described previously[78]. Flow cytometry was performed at the MUSC FACS core facility using BD Fortessa X-20 Analytic Flow Cytometer (BD Biosciences) to detect annexin V- and/or PI-bound cells. Apoptotic cells were defined as annexin V positive and PI negative.

### Statistics:

Each data set is presented as mean±SEM. All the statistical analysis was performed using the GraphPad Prism 7 software. The Mann-Whitney test (nonparametric test) was performed to assess the statistical differences between two groups, whereas to analyze statistical differences between more than two groups, 1-way (Kruskal-Wallis test) or 2-way ANOVA (Sidak's multiple comparison test) nonparametric analysis of variance were performed. Details of the statistical analyses used for each experiment are provided in the respective figure legends. A p value of $\leq 0.05$ was considered as statistically significant.

### Human and animal Study approval:

Human studies were approved by the Institutional review board, MUSC (IRB # 18380 and POSEIDON # 19764). All animal studies were conducted as per the protocol approved by the University of Pennsylvania and MUSC, Institutional Animal Care and Use Committee and NIH guidelines for the Care and Use of Laboratory Animals (Protocol # IACUC-2018–00360). Treatment of mice, including housing, injections and surgery was in accordance with the institutional guidelines. Isoflurane anesthesia (5% induction, 2% maintenance), and perioperative buprenorphine was used to perform all surgeries.

## Supplementary Material

Refer to Web version on PubMed Central for supplementary material.

## ACKNOWLEDGEMENTS

National Institutes of Health, NIDDK, Grant RO1 2R01DK087956–06A1 and R56 DK116887–01A1 to D. N. are duly acknowledged. Carl Gottschalk award to S.-H. K and Ben J. Lipps Research Fellowship to A.K.S from American Society of Nephrology are also acknowledged. We thank Babita Kumari for technical assistance in the laboratory.

**Sources of support:** This work was supported in whole or in part by the NIH and NIDDK Grants, 2R01DK087956–06A1 and R56 DK116887–01A1 to D. N, and American Society of Nephrology for Carl Gottschalk award to S.-H. K and Ben J. Lipps Research Fellowship to A.K.S.

## REFERENCES

1. Kerjaschki D, Caught flat-footed: podocyte damage and the molecular bases of focal glomerulosclerosis. J Clin Invest. 108:1583–1587, 2001 [PubMed: 11733553]
2. Mundel P and Shankland SJ, Podocyte biology and response to injury. J Am Soc Nephrol. 13:3005–3015, 2002 [PubMed: 12444221]
3. Shankland SJ, The podocyte's response to injury: role in proteinuria and glomerulosclerosis. Kidney Int. 69:2131–2147, 2006 [PubMed: 16688120]
4. Cellesi F, Li M, and Rastaldi MP, Podocyte injury and repair mechanisms. Curr Opin Nephrol Hypertens. 24:239–244, 2015 [PubMed: 26066473]
5. Nagata M, Podocyte injury and its consequences. Kidney Int. 89:1221–1230, 2016 [PubMed: 27165817]
6. Schiffer M, Bitzer M, Roberts IS, Kopp JB, ten Dijke P, Mundel P, et al., Apoptosis in podocytes induced by TGF-beta and Smad7. J Clin Invest. 108:807–816, 2001 [PubMed: 11560950]
7. Peters I, Tossidou I, Achenbach J, Woroniecki R, Mengel M, Park JK, et al., IGF-binding protein-3 modulates TGF-beta/BMP-signaling in glomerular podocytes. J Am Soc Nephrol. 17:1644–1656, 2006 [PubMed: 16672319]
8. Kim JH, Kim BK, Moon KC, Hong HK, and Lee HS, Activation of the TGF-beta/Smad signaling pathway in focal segmental glomerulosclerosis. Kidney Int. 64:1715–1721, 2003 [PubMed: 14531804]
9. Loeffler I and Wolf G, Transforming growth factor-beta and the progression of renal disease. Nephrol Dial Transplant. 29 Suppl 1:i37–i45, 2014 [PubMed: 24030832]
10. Gillespie PG, Albanesi JP, Bahler M, Bement WM, Berg JS, Burgess DR, et al., Myosin-I nomenclature. J Cell Biol. 155:703–704, 2001 [PubMed: 11724811]
11. Gillespie PG, Myosin I and adaptation of mechanical transduction by the inner ear. Philos Trans R Soc Lond B Biol Sci. 359:1945–1951, 2004 [PubMed: 15647170]
12. Barylko B, Jung G, and Albanesi JP, Structure, function, and regulation of myosin 1C. Acta Biochim Pol. 52:373–380, 2005 [PubMed: 15933767]
13. Brandstaetter H, Kendrick-Jones J, and Buss F, Myo1c regulates lipid raft recycling to control cell spreading, migration and Salmonella invasion. J Cell Sci. 125:1991–2003, 2012 [PubMed: 22328521]
14. Bose A, Guilherme A, Robida SI, Nicoloro SM, Zhou QL, Jiang ZY, et al., Glucose transporter recycling in response to insulin is facilitated by myosin Myo1c. Nature. 420:821–824, 2002 [PubMed: 12490950]
15. Wagner MC, Barylko B, and Albanesi JP, Tissue distribution and subcellular localization of mammalian myosin I. J Cell Biol. 119:163–170, 1992 [PubMed: 1527166]
16. Fan Y, Eswarappa SM, Hitomi M, and Fox PL, Myo1c facilitates G-actin transport to the leading edge of migrating endothelial cells. J Cell Biol. 198:47–55, 2012 [PubMed: 22778278]
17. Venit T, Dzijak R, Kalendova A, Kahle M, Rohozkova J, Schmidt V, et al., Mouse nuclear myosin I knock-out shows interchangeability and redundancy of myosin isoforms in the cell nucleus. PLoS One. 8:e61406, 2013 [PubMed: 23593477]
18. Arif E, Wagner MC, Johnstone DB, Wong HN, George B, Pruthi PA, et al., Motor protein Myo1c is a podocyte protein that facilitates the transport of slit diaphragm protein Neph1 to the podocyte membrane. Mol Cell Biol. 31:2134–2150, 2011 [PubMed: 21402783]

19. Brandstaetter H, Kishi-Itakura C, Tumbarello DA, Manstein DJ, and Buss F, Loss of functional MYO1C/myosin 1c, a motor protein involved in lipid raft trafficking, disrupts autophagosome-lysosome fusion. Autophagy. 10:2310–2323, 2014 [PubMed: 25551774]
20. Philimonenko VV, Zhao J, Iben S, Dingova H, Kysela K, Kahle M, et al., Nuclear actin and myosin I are required for RNA polymerase I transcription. Nat Cell Biol. 6:1165–1172, 2004 [PubMed: 15558034]
21. Pierchala BA, Munoz MR, and Tsui CC, Proteomic analysis of the slit diaphragm complex: CLIC5 is a protein critical for podocyte morphology and function. Kidney Int. 78:868–882, 2010 [PubMed: 20664558]
22. Zattelman L, Regev R, Usaj M, Reinke PYA, Giese S, Samson AO, et al., N-terminal splicing extensions of the human MYO1C gene fine-tune the kinetics of the three full-length myosin IC isoforms. J Biol Chem 2017
23. Boguslavsky S, Chiu T, Foley KP, Osorio-Fuentealba C, Antonescu CN, Bayer KU, et al., Myo1c binding to submembrane actin mediates insulin-induced tethering of GLUT4 vesicles. Mol Biol Cell. 23:4065–4078, 2012 [PubMed: 22918957]
24. Nagy A, Cre recombinase: the universal reagent for genome tailoring. Genesis. 26:99–109, 2000 [PubMed: 10686599]
25. Muzumdar MD, Tasic B, Miyamichi K, Li L, and Luo L, A global double-fluorescent Cre reporter mouse. Genesis. 45:593–605, 2007 [PubMed: 17868096]
26. Velez JCQ, Arif E, Rodgers J, Hicks MP, Arthur JM, Nihalani D, et al., Deficiency of the Angiotensinase Aminopeptidase A Increases Susceptibility to Glomerular Injury. J Am Soc Nephrol. 28:2119–2132, 2017 [PubMed: 28202497]
27. Arif E, Solanki AK, and Nihalani D, Adriamycin susceptibility among C57BL/6 substrains. Kidney Int. 89:721–723, 2016
28. Wang Y, Wang YP, Tay YC, and Harris DC, Progressive adriamycin nephropathy in mice: sequence of histologic and immunohistochemical events. Kidney Int. 58:1797–1804, 2000 [PubMed: 11012915]
29. Johnstone DB and Holzman LB, Clinical impact of research on the podocyte slit diaphragm. Nat Clin Pract Nephrol. 2:271–282, 2006 [PubMed: 16932440]
30. Tryggvason K, Patrakka J, and Wartiovaara J, Hereditary proteinuria syndromes and mechanisms of proteinuria. N Engl J Med. 354:1387–1401, 2006 [PubMed: 16571882]
31. Barletta GM, Kovari IA, Verma RK, Kerjaschki D, and Holzman LB, Nephrin and Neph1 colocalize at the podocyte foot process intercellular junction and form cis hetero-oligomers. J Biol Chem. 278:19266–19271, 2003 [PubMed: 12646566]
32. Wagner MC, Rhodes G, Wang E, Pruthi V, Arif E, Saleem MA, et al., Ischemic injury to kidney induces glomerular podocyte effacement and dissociation of slit diaphragm proteins Neph1 and ZO-1. J Biol Chem. 283:35579–35589, 2008 [PubMed: 18922801]
33. Verma R, Kovari I, Soofi A, Nihalani D, Patrie K, and Holzman LB, Nephrin ectodomain engagement results in Src kinase activation, nephrin phosphorylation, Nck recruitment, and actin polymerization. J Clin Invest. 116:1346–1359, 2006 [PubMed: 16543952]
34. Garg P, Verma R, Nihalani D, Johnstone DB, and Holzman LB, Neph1 cooperates with nephrin to transduce a signal that induces actin polymerization. Mol Cell Biol. 27:8698–8712, 2007 [PubMed: 17923684]
35. Lichtnekert J, Kulkarni OP, Mulay SR, Rupanagudi KV, Ryu M, Allam R, et al., Anti-GBM glomerulonephritis involves IL-1 but is independent of NLRP3/ASC inflammasome-mediated activation of caspase-1. PLoS One. 6:e26778, 2011 [PubMed: 22046355]
36. George B, Verma R, Soofi AA, Garg P, Zhang J, Park TJ, et al., Crk1/2-dependent signaling is necessary for podocyte foot process spreading in mouse models of glomerular disease. J Clin Invest. 122:674–692, 2012 [PubMed: 22251701]
37. Meng XM, Nikolic-Paterson DJ, and Lan HY, Inflammatory processes in renal fibrosis. Nat Rev Nephrol. 10:493–503, 2014 [PubMed: 24981817]
38. Finer G, Schnaper HW, Kanwar YS, Liang X, Lin HY, and Hayashida T, Divergent roles of Smad3 and PI3-kinase in murine adriamycin nephropathy indicate distinct mechanisms of proteinuria and fibrogenesis. Kidney Int. 82:525–536, 2012 [PubMed: 22534961]

39. Chevalier RL, Forbes MS, and Thornhill BA, Ureteral obstruction as a model of renal interstitial fibrosis and obstructive nephropathy. Kidney Int. 75:1145–1152, 2009 [PubMed: 19340094]
40. Wu YL, Xie J, An SW, Oliver N, Barrezueta NX, Lin MH, et al., Inhibition of TRPC6 channels ameliorates renal fibrosis and contributes to renal protection by soluble klotho. Kidney Int. 91:830–841, 2017 [PubMed: 27979597]
41. Fu P, Liu F, Su S, Wang W, Huang XR, Entman ML, et al., Signaling mechanism of renal fibrosis in unilateral ureteral obstructive kidney disease in ROCK1 knockout mice. J Am Soc Nephrol. 17:3105–3114, 2006 [PubMed: 17005937]
42. Satoh M, Nagasu H, Morita Y, Yamaguchi TP, Kanwar YS, and Kashihara N, Klotho protects against mouse renal fibrosis by inhibiting Wnt signaling. Am J Physiol Renal Physiol. 303:F1641–1651, 2012 [PubMed: 23034937]
43. Bottinger EP and Bitzer M, TGF-beta signaling in renal disease. J Am Soc Nephrol. 13:26002610, 2002
44. Meng XM, Nikolic-Paterson DJ, and Lan HY, TGF-beta: the master regulator of fibrosis. Nat Rev Nephrol. 12:325–338, 2016 [PubMed: 27108839]
45. Liu Y, Cellular and molecular mechanisms of renal fibrosis. Nat Rev Nephrol. 7:684–696, 2011 [PubMed: 22009250]
46. Eddy AA, Overview of the cellular and molecular basis of kidney fibrosis. Kidney Int Suppl (2011). 4:2–8, 2014 [PubMed: 25401038]
47. Almuzzaini B, Sarshad AA, Farrants AK, and Percipalle P, Nuclear myosin 1 contributes to a chromatin landscape compatible with RNA polymerase II transcription activation. BMC Biol. 13:35, 2015 [PubMed: 26044184]
48. Nevzorov I, Sidorenko E, Wang W, Zhao H, and Vartiainen MK, Myosin-1C uses a novel phosphoinositide-dependent pathway for nuclear localization. EMBO Rep 2018
49. Osada M, Park HL, Park MJ, Liu JW, Wu G, Trink B, et al., A p53-type response element in the GDF15 promoter confers high specificity for p53 activation. Biochem Biophys Res Commun. 354:913–918, 2007 [PubMed: 17276395]
50. Corre J, Hebraud B, and Bourin P, Concise review: growth differentiation factor 15 in pathology: a clinical role? Stem Cells Transl Med. 2:946–952, 2013 [PubMed: 24191265]
51. Adela R and Banerjee SK, GDF-15 as a Target and Biomarker for Diabetes and Cardiovascular Diseases: A Translational Prospective. J Diabetes Res. 2015:490842, 2015 [PubMed: 26273671]
52. Huang Z, Zhang L, Chen Y, Zhang H, Yu C, Zhou F, et al., RhoA deficiency disrupts podocyte cytoskeleton and induces podocyte apoptosis by inhibiting YAP/dendrin signal. BMC Nephrol. 17:66, 2016 [PubMed: 27389190]
53. Arif E, Kumari B, Wagner MC, Zhou W, Holzman LB, and Nihalani D, Myo1c is an unconventional myosin required for zebrafish glomerular development. Kidney Int 2013
54. Krendel M, Osterweil EK, and Mooseker MS, Myosin 1E interacts with synaptojanin-1 and dynamin and is involved in endocytosis. FEBS Lett. 581:644–650, 2007 [PubMed: 17257598]
55. Mele C, Iatropoulos P, Donadelli R, Calabria A, Maranta R, Cassis P, et al., MYO1E mutations and childhood familial focal segmental glomerulosclerosis. N Engl J Med. 365:295–306, 2011 [PubMed: 21756023]
56. Blattner SM, Hodgin JB, Nishio M, Wylie SA, Saha J, Soofi AA, et al., Divergent functions of the Rho GTPases Rac1 and Cdc42 in podocyte injury. Kidney Int. 84:920–930, 2013 [PubMed: 23677246]
57. Yu H, Suleiman H, Kim AH, Miner JH, Dani A, Shaw AS, et al., Rac1 activation in podocytes induces rapid foot process effacement and proteinuria. Mol Cell Biol. 33:4755–4764, 2013 [PubMed: 24061480]
58. Guzman J, Jauregui AN, Merscher-Gomez S, Maiguel D, Muresan C, Mitrofanova A, et al., Podocyte-specific GLUT4-deficient mice have fewer and larger podocytes and are protected from diabetic nephropathy. Diabetes. 63:701–714, 2014 [PubMed: 24101677]
59. Greka A and Mundel P, Cell biology and pathology of podocytes. Annu Rev Physiol. 74:299–323, 2012 [PubMed: 22054238]
60. Abrahamson DR, Role of the podocyte (and glomerular endothelium) in building the GBM. Semin Nephrol. 32:342–349, 2012 [PubMed: 22958488]

61. Jourdan T, Park JK, Varga ZV, Paloczi J, Coffey NJ, Rosenberg AZ, et al., Cannabinoid-1 receptor deletion in podocytes mitigates both glomerular and tubular dysfunction in a mouse model of diabetic nephropathy. Diabetes Obes Metab. 20:698–708, 2018 [PubMed: 29106063]
62. Kramer E and Clancy JP, TGFbeta as a therapeutic target in cystic fibrosis. Expert Opin Ther Targets 2017
63. Varga J and Pasche B, Transforming growth factor beta as a therapeutic target in systemic sclerosis. Nat Rev Rheumatol. 5:200–206, 2009 [PubMed: 19337284]
64. Neuzillet C, Tijeras-Raballand A, Cohen R, Cros J, Faivre S, Raymond E, et al., Targeting the TGFbeta pathway for cancer therapy. Pharmacol Ther. 147:22–31, 2015 [PubMed: 25444759]
65. Liang X, Schnaper HW, Matsusaka T, Pastan I, Ledbetter S, and Hayashida T, Anti-TGF-beta Antibody, 1D11, Ameliorates Glomerular Fibrosis in Mouse Models after the Onset of Proteinuria. PLoS One. 11:e0155534, 2016 [PubMed: 27187580]
66. Nakamori Y, Emoto M, Fukuda N, Taguchi A, Okuya S, Tajiri M, et al., Myosin motor Myo1c and its receptor NEMO/IKK-gamma promote TNF-alpha-induced serine307 phosphorylation of IRS-1. J Cell Biol. 173:665–671, 2006 [PubMed: 16754954]
67. Johnen H, Lin S, Kuffner T, Brown DA, Tsai VW, Bauskin AR, et al., Tumor-induced anorexia and weight loss are mediated by the TGF-beta superfamily cytokine MIC-1. Nat Med. 13:13331340, 2007
68. Ponticos M, Harvey C, Ikeda T, Abraham D, and Bou-Gharios G, JunB mediates enhancer/promoter activity of COL1A2 following TGF-beta induction. Nucleic Acids Res. 37:5378–5389, 2009 [PubMed: 19561194]
69. Breit SN, Tsai VW, and Brown DA, Targeting Obesity and Cachexia: Identification of the GFRAL Receptor-MIC-1/GDF15 Pathway. Trends Mol Med. 23:1065–1067, 2017 [PubMed: 29129392]
70. Nair N and Gongora E, Correlations of GDF-15 with sST2, MMPs, and worsening functional capacity in idiopathic dilated cardiomyopathy: Can we gain new insights into the pathophysiology? J Circ Biomark. 7:1849454417751735, 2018
71. Geurts N, Martens E, Verhenne S, Lays N, Thijs G, Magez S, et al., Insufficiently defined genetic background confounds phenotypes in transgenic studies as exemplified by malaria infection in Tlr9 knockout mice. PLoS One. 6:e27131, 2011 [PubMed: 22096530]
72. Terryn S, Jouret F, Vandenabeele F, Smolders I, Moreels M, Devuyst O, et al., A primary culture of mouse proximal tubular cells, established on collagen-coated membranes. Am J Physiol Renal Physiol. 293:F476–485, 2007 [PubMed: 17475898]
73. Saleem MA, Ni L, Witherden I, Tryggvason K, Ruotsalainen V, Mundel P, et al., Colocalization of nephrin, podocin, and the actin cytoskeleton: evidence for a role in podocyte foot process formation. Am J Pathol. 161:1459–1466, 2002 [PubMed: 12368218]
74. Lloyd CM, Minto AW, Dorf ME, Proudfoot A, Wells TN, Salant DJ, et al., RANTES and monocyte chemoattractant protein-1 (MCP-1) play an important role in the inflammatory phase of crescentic nephritis, but only MCP-1 is involved in crescent formation and interstitial fibrosis. J Exp Med. 185:1371–1380, 1997 [PubMed: 9104823]
75. Mohanty BK and Bastia D, Binding of the replication terminator protein Fob1p to the Ter sites of yeast causes polar fork arrest. J Biol Chem. 279:1932–1941, 2004 [PubMed: 14576157]
76. Zaman S, Choudhury M, Jiang JC, Srivastava P, Mohanty BK, Danielson C, et al., Mechanism of Regulation of Intrachromatid Recombination and Long-Range Chromosome Interactions in Saccharomyces cerevisiae. Mol Cell Biol. 36:1451–1463, 2016 [PubMed: 26951198]
77. Schaldecker T, Kim S, Tarabanis C, Tian D, Hakroush S, Castonguay P, et al., Inhibition of the TRPC5 ion channel protects the kidney filter. J Clin Invest. 123:5298–5309, 2013 [PubMed: 24231357]
78. Lee HW, Arif E, Altintas MM, Quick K, Maheshwari S, Plezia A, et al., High-content screening assay-based discovery of paullones as novel podocyte-protective agents. Am J Physiol Renal Physiol. 314:F280–F292, 2018 [PubMed: 29046299]

## TRANSLATIONAL STATEMENT

The past decade has seen exponential growth in our understanding of the podocyte biology, yet effective therapies to prevent podocytopathies remains elusive. This is primarily because of our insufficient understanding of the molecular mechanisms that are involved in preventing injury-mediated loss of podocyte structural and function. Fibrosis is a common outcome in various podocytopathies, which is associated with total loss of renal filtration function and can be induced either by drugs or environmental factors. Transforming growth factor-β (TGF-β), a profibrotic cytokine that has been shown to play a pivotal role in a variety of pathological events including, fibrosis and sclerosis of glomeruli leading to impaired glomerular function and ESRD. While the effects of TGF-β are pleotropic, the molecular mechanisms that regulate TGF-β signaling may define the pathological outcomes induced by TGF-β. The results presented in this study demonstrate Myo1c as a novel regulator of TGF-β signaling whose specific loss in podocytes, prevented mice glomeruli from developing fibrotic lesions in response to glomerular injury. Thus, understanding how Myo1c participates in regulating response of podocytes to TGF-β, may lead to identifying novel therapeutic targets in treating podocytopathies. One such novel target identified in this study is GDF15.

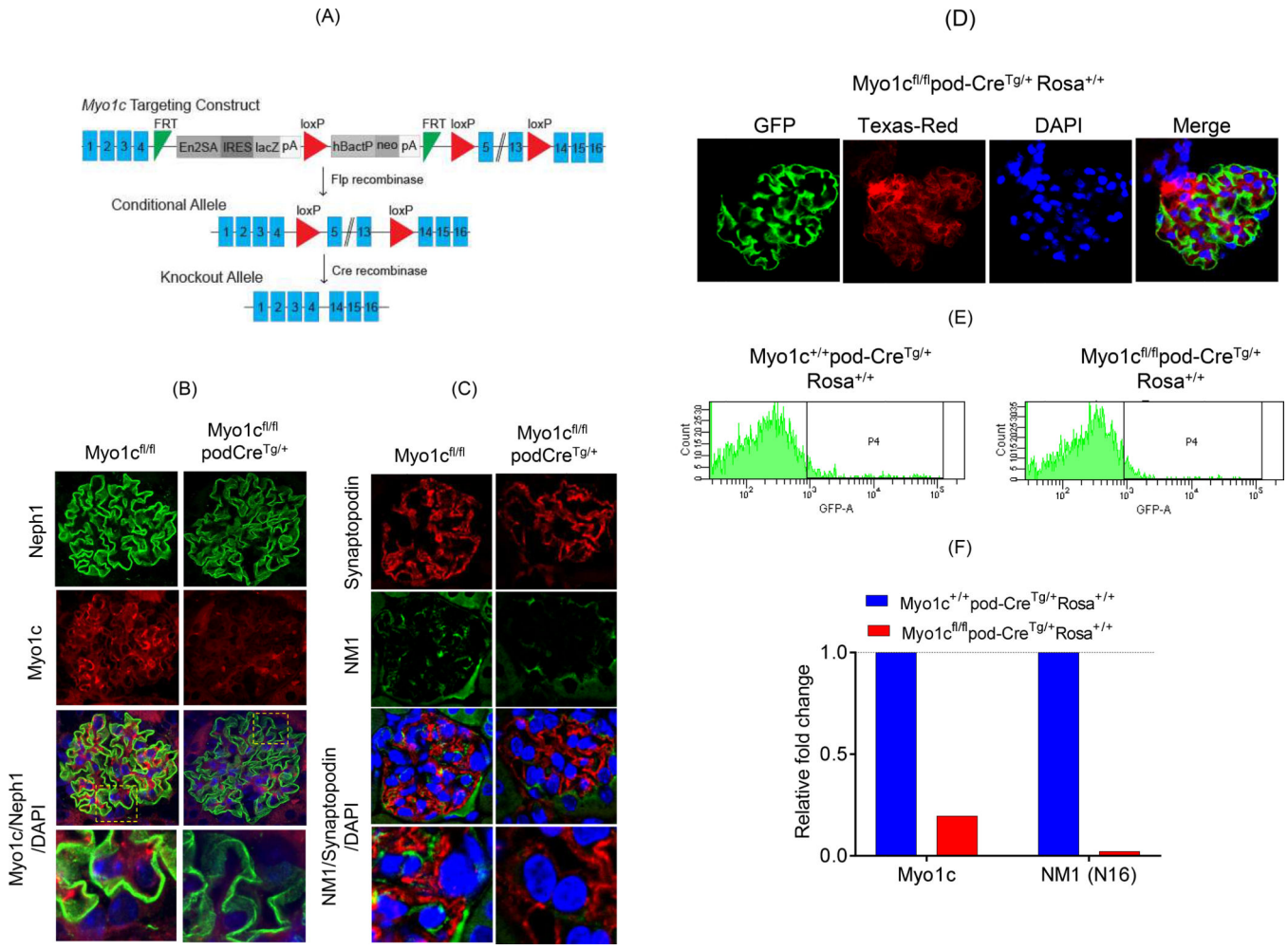


**Figure 1: Construction of podocyte-specific Myo1c null mice:**

(**A**) Schematic diagram of Myo1c targeting vector shows deletion of Myo1c Exons 5–13 following cre recombination. (**B**) Podocyte-specific deletion of Myo1c was confirmed by staining of paraffin-embedded mouse kidney sections from Myo1c$^{fl/fl}$ (control) and Myo1c$^{fl/fl}$pod- Cre$^{Tg/+}$ mice using Neph1 (green) and Myo1c (Red) antibodies and DAPI (Blue). The images were collected using an confocal microscope. Immunofluorescence staining confirm deletion of Myo1c protein in podocytes (marked with arrows). Scale bars: 20μm (**C**) Podocyte-specific deletion of Myo1c was confirmed by staining with NM1 (green) and synaptopodin (Red) antibodies and DAPI (Blue). The images were collected using confocal microscopy. Scale bars: 20μm. **(D)** Myo1c$^{fl/fl}$pod-Cre$^{Tg/+}$ or Myo1c$^{+/+}$pod-Cre$^{Tg/+}$ mice were crossed with ROSA$^{mT/mG}$ mice to generate GFP expressing podocytes, while all the other cell types remained red (Texas-red). **(E)** The green podocytes were separated by FACS sorting (~40000–50000 cells were obtained from glomeruli isolated from kidneys of 3 mice each). **(F)** qPCR analysis of isolated podocytes showed more than 90% reduction in cytoplasmic and nuclear Myo1c expression.

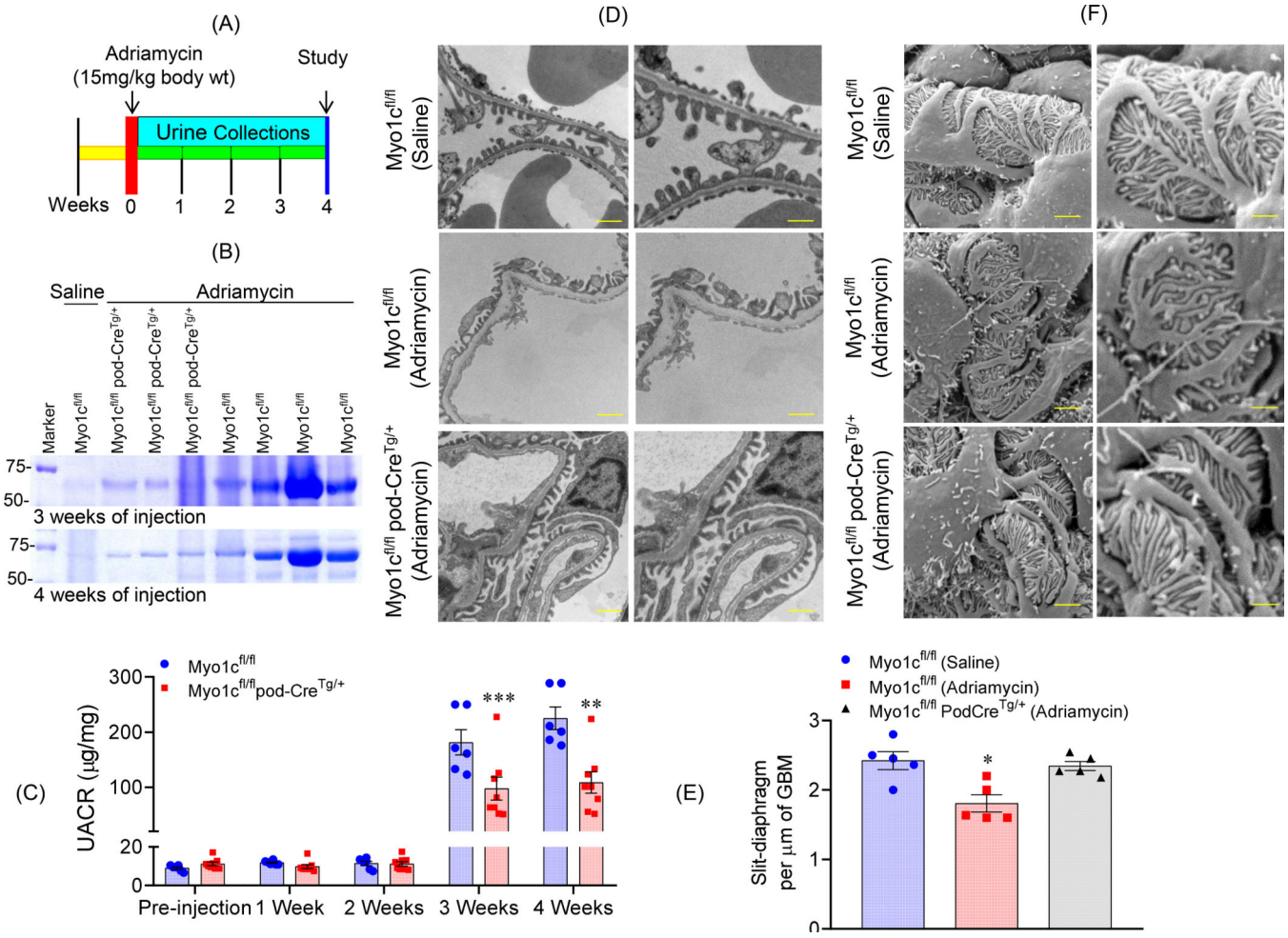


**Figure 2: Podocyte specific Myo1c deletion protects mice from adriamycin induced podocytopathy:**

**(A)**. Experimental timeline of adriamycin injection and urine collections. (**B**). Adriamycin sensitivity was tested in Myo1c$^{fl/fl}$ and Myo1c$^{fl/fl}$pod-Cre$^{Tg/+}$ mice on adriamycin sensitive C57BL/6N background. The SDS-PAGE analysis of 3 and 4 weeks post adriamycin injection urine samples showed heavy albuminuria in Myo1c$^{fl/fl}$ mice but not in Myo1c$^{fl/fl}$pod-Cre$^{Tg/+}$ mice. (**C**) The albumin/creatinine analysis further showed significant reduction in adriamycin-induced albuminuria in Myo1c$^{fl/fl}$pod-Cre$^{Tg/+}$ mice. ***$P \leq 0.001$, **$P \leq 0.01$ vs. Myo1c$^{fl/fl}$, 2-way ANOVA (Sidak's multiple comparison test). Myo1c$^{fl/fl}$, n=6 mice and Myo1c$^{fl/fl}$pod-Cre$^{Tg/+}$, n=9 mice. Data presented in means±SEM. (**D**) Adriamycin-induced damages were assessed by TEM analysis of kidney sections, which showed areas of flattening with significant shortening and fusion of podocyte foot processes and loss of slit diaphragm in control Myo1c$^{fl/fl}$ mice, whereas the podocytes of Myo1c$^{fl/fl}$pod-Cre$^{Tg/+}$ or saline treated control mice were largely healthy. Scale bars: 1µm (Left panel); 500nm (Right panel). (**E**) Quantitative analysis of electron micrographs showed significant reduction in the number of slit-diaphragm/µm in adriamycin treated Myo1c$^{fl/fl}$ mice but not in Myo1c$^{fl/fl}$pod-Cre$^{Tg/+}$ or saline treated control mice. *$P \leq 0.05$ vs Myo1c$^{fl/fl}$ (Saline) and Myo1c$^{fl/fl}$pod-Cre$^{Tg/+}$ (Adriamycin), one-way ANOVA (Kruskal-Wallis test), Multiple scoring of each

animal was first averaged and the average value of each animal was used for constructing graphs and statistical analysis. n=5 mice in each group, The bar graphs represent mean ±SEM. (**F**) SEM analysis showed flattening of podocytes in adriamycin treated Myo1c$^{fl/fl}$. Scale bars: 2μm (Left panel); 1μm (Right panel).

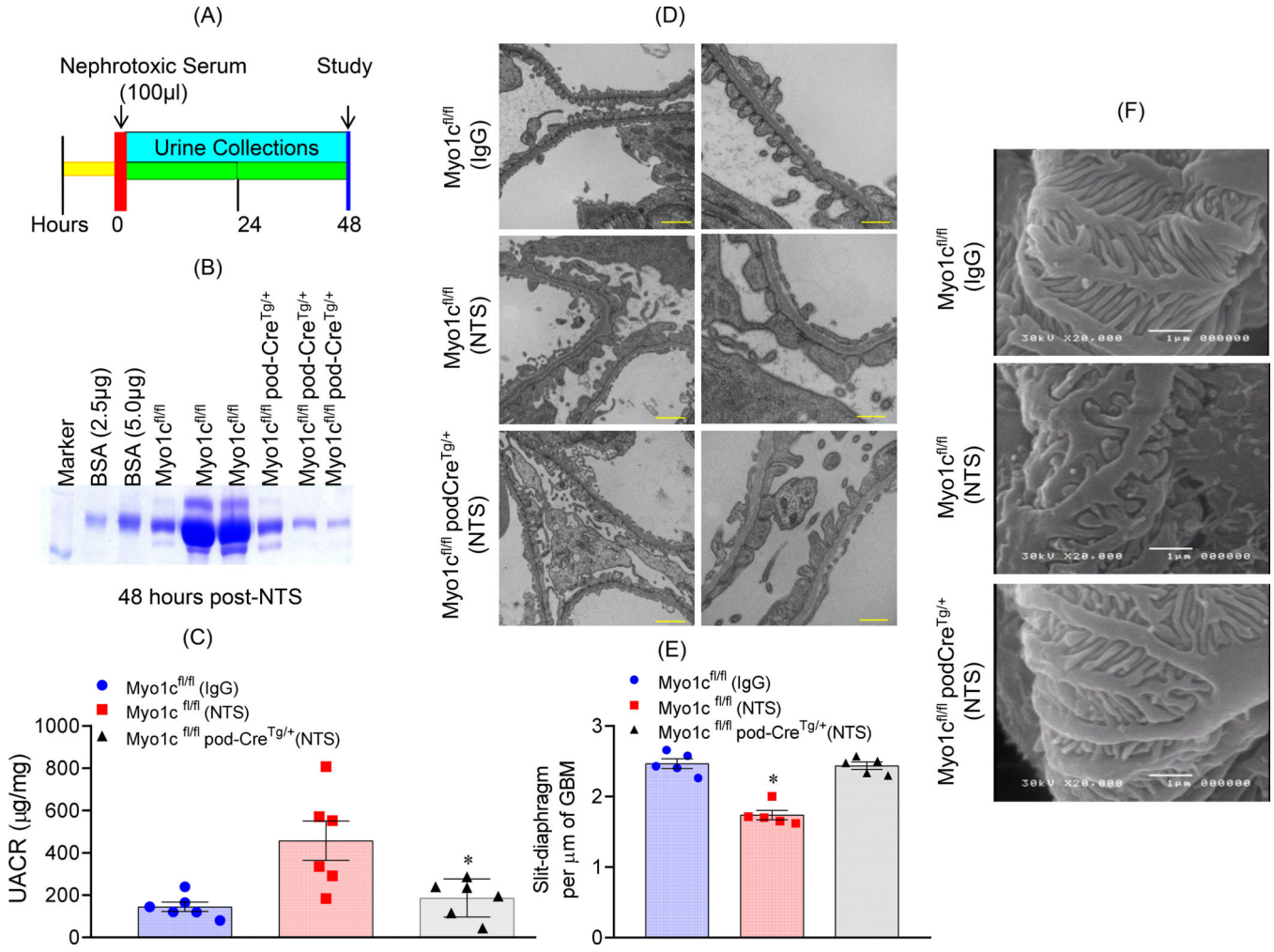


**Figure 3: Podocyte-specific Myo1c deletion protects mice from NTS-induced podocytopathy:**

**(A)** Experimental timeline of NTS injection and urine collections. (**B**) SDS-PAGE and (**C**) albumin creatinine analysis and showed albuminuria was significantly reduced in Myo1c$^{fl/fl}$pod-Cre$^{Tg/+}$ mice, when compared to the Myo1c$^{fl/fl}$ mice. *$P$≤0.05 vs Myo1c$^{fl/fl}$ (NTS), one-way ANOVA (Kruskal-Wallis test), n=6 mice per group. Data presented in means±SEM. (**D-F**) The microscopic analysis (SEM and TEM) of kidney sections showed significant podocytes flattening and increased foot process fusion with loss of slit diaphragm in NTS treated Myo1c$^{fl/fl}$ mice but not in Myo1c$^{fl/fl}$pod- Cre$^{Tg/+}$ or sheep IgG treated mice. (**E**) Quantitative analysis of TEM images showed numbers of slit-diaphragm per micrometer of GBM were reduced in NTS treated Myo1c$^{fl/fl}$ mice. *$P$≤0.05 vs Myo1c$^{fl/fl}$ (NTS), one-way ANOVA (Kruskal-Wallis test), Multiple scoring of each animal was first averaged and the average value of each animal was used for constructing graphs and statistical analysis. n=5 mice in each group. Data presented in mean±SEM. Scale bars: 800nm (D, Left panel); 200nm (D, Right panel); 1 µm (F).

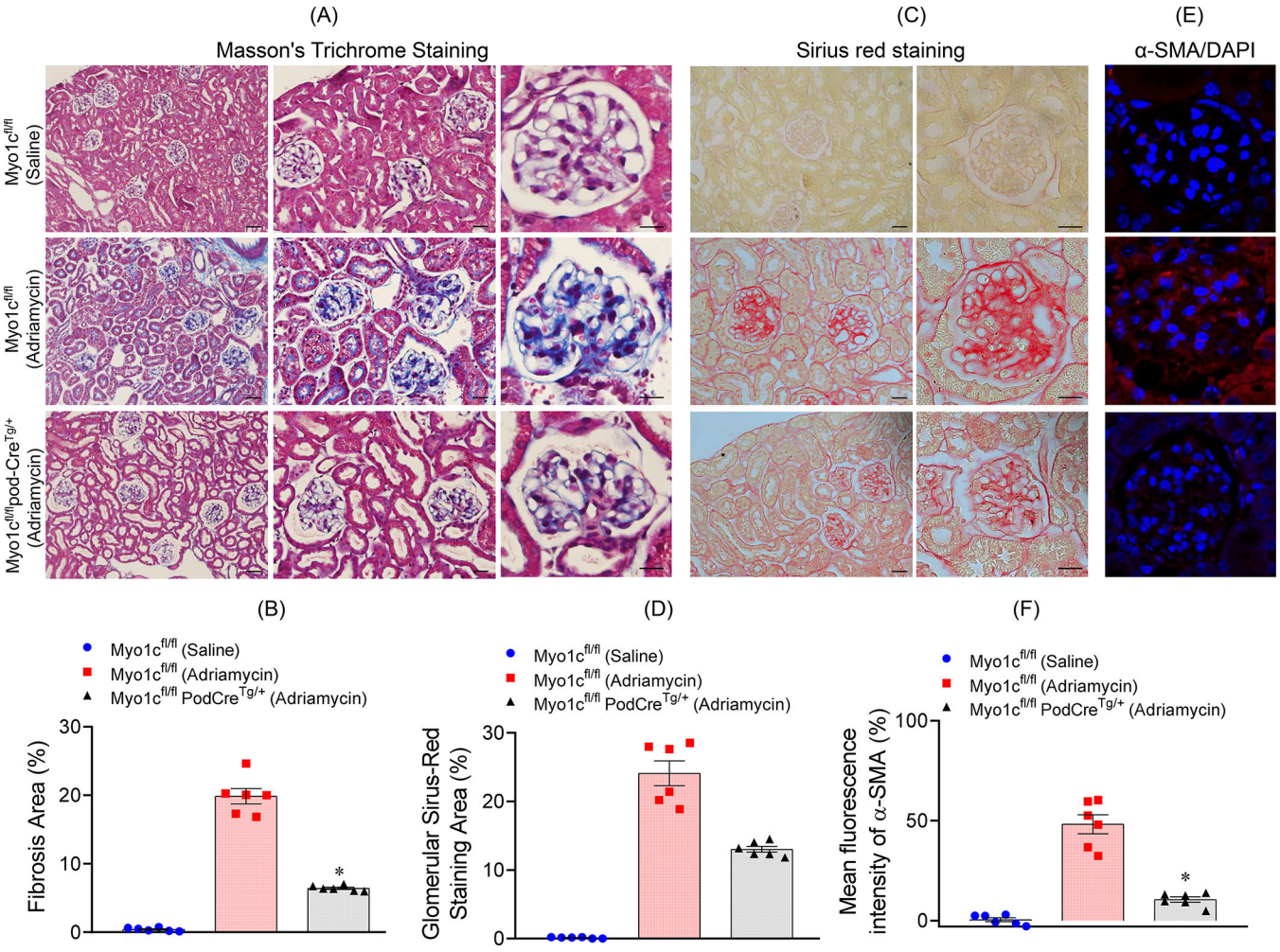


**Figure 4: Podocyte-specific Myo1c null mice were protected from adriamycin induced renal fibrosis:**

Glomerular fibrosis in adriamycin treated Myo1c$^{fl/fl}$ and Myo1c$^{fl/fl}$pod-Cre$^{Tg/+}$ mice was assessed using Masson's trichrome and Sirius red stainings. (**A**) Increased Masson's trichrome staining was noted in the glomeruli of Myo1c$^{fl/fl}$ mice. Scale bars: left panel, 100μm; middle panel 50μm and right panel 20μm. (**B**) Fibrotic area assessment from the Masson's trichrome stained glomeruli of Myo1c$^{fl/fl}$ mice showed ~20% fibrosis, whereas the Myo1c$^{fl/fl}$pod-Cre$^{Tg/+}$ showed ~6% fibrosis. *$P$≤0.05 vs Myo1c$^{fl/fl}$ (Adriamycin), one-way ANOVA (Kruskal-Wallis test), n=6 mice in each group using manual outlining method. Data presented in mean±SEM. **(C)** Similar to Masson's trichrome, the Sirius red staining was also elevated in Myo1c$^{fl/fl}$ mice glomeruli. Scale bars: left panel, 50μm and right panel 20μm. **(D)** Quantitative assessment using five glomeruli from six mice in each group showed significantly increased fibrotic areas in Myo1c$^{fl/fl}$ mice, when compared to Myo1c$^{fl/fl}$pod-Cre$^{Tg/+}$ mice. </P/> *$P$≤0.05 vs Myo1c$^{fl/fl}$ (Adriamycin), one-way ANOVA (Kruskal-Wallis test), n=6 mice in each group. Data presented in means±SEM. **(E)** Immunostaining of kidney sections using α-SMA antibody and DAPI (blue) showed increased α-SMA expression in Myo1c$^{fl/fl}$ mice in response to injury. Scale bars: 20μm **(F)** Quantitative analysis of immunofluorescence images showed that injury-induced α-SMA expression was

elevated in Myo1c$^{fl/fl}$ mice when compared to Myo1c$^{fl/fl}$pod-Cre$^{Tg/+}$ mice. *$P \leq 0.05$ vs Myo1c$^{fl/fl}$ (Adriamycin), one-way ANOVA (Kruskal-Wallis test), n=6 mice in each group. Data presented in mean±SEM.

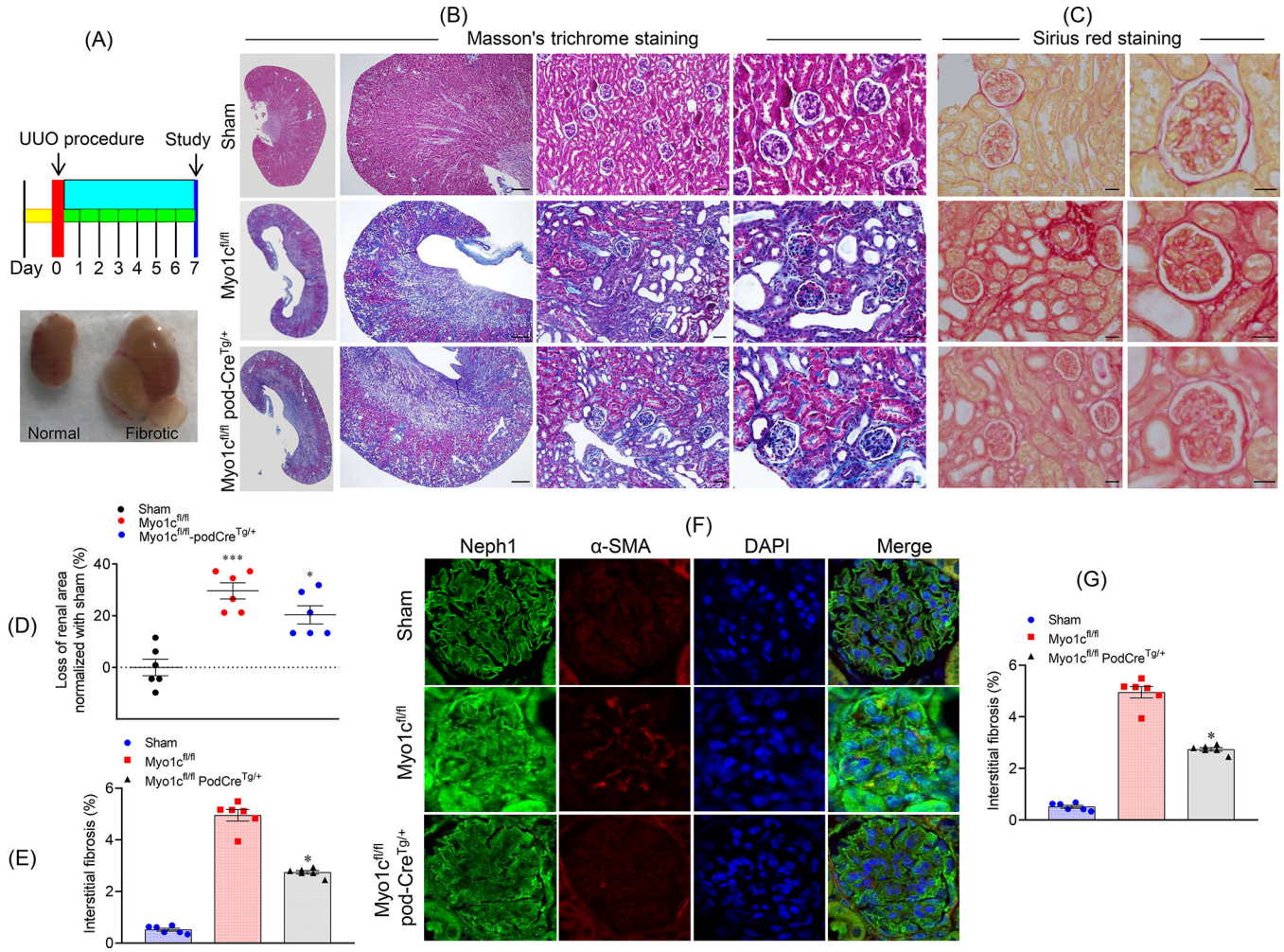


**Figure 5: Podocyte-specific Myo1c deletion attenuates post-UUO renal fibrosis:**

(**A**) Experimental timeline of UUO procedure (upper panel) and representative image of non-obstructed right kidney (left panel) and obstructed left kidney (right panel). **(B)** Representative macrophotographs (increasing magnification) of Masson-stained kidney sections from sham and day 7 post-UUO procedure performed on, Myo1c$^{fl/fl}$ and Myo1c$^{fl/fl}$pod-Cre$^{Tg/+}$ mice are shown (left panel). Scale bars: left panel, 200μm; middle panel 100μm and right panel 50μm. n=6 mice in each group. (**C**) Representative images of stained kidney sections show increased Sirius red staining in Myo1c$^{fl/fl}$ mice as compared to the Myo1c$^{fl/fl}$pod-Cre$^{Tg/+}$ and sham operated mice. Images were collected at 40x magnification and enlarged glomerular regions are presented in the right panel. Scale bars: left panel 50μm and right panel 20μm. (**D**) Reduction in total renal area (% area, normalized with sham) post UUO procedure was quantitatively assessed and showed ~30% reduction in Myo1c$^{fl/fl}$, whereas in Myo1c$^{fl/fl}$pod-Cre$^{Tg/+}$ mice ~20% reduction was noted. ***$P$=0.0001, *P<0.05, vs Sham, one-way ANOVA (Kruskal-Wallis test). Data presented in mean±SEM. n=6 mice in each group. (**E**) Quantitative analysis of interstitial fibrosis using Masson's trichrome staining showed that fibrosis increased by ~6% in Myo1c$^{fl/fl}$ renal tissue, whereas in Myo1c$^{fl/fl}$pod-Cre$^{Tg/+}$ mice only ~2% increase was observed. *$P$≤0.05, Myo1c$^{fl/fl}$ (UUO) vs Myo1c$^{fl/fl}$pod-Cre$^{Tg/+}$ (UUO), one-way ANOVA (Kruskal-Wallis test). Data presented as

mean±SEM. n=6 mice in each group. **(F)** Representative confocal images from Myo1c$^{fl/fl}$ and Myo1c$^{fl/fl}$pod-Cre$^{Tg/+}$ mice immunostained with α-SMA (Red) and Neph1 (Green) antibodies and DAPI (Blue) are shown. Scale bars: 20μm. (**G**) Bar graphs represent mean fluorescent intensity of α- SMA staining. *$P$≤0.05, Myo1c$^{fl/fl}$ (UUO) vs Myo1c$^{fl/fl}$pod-Cre$^{Tg/+}$ (UUO), one-way ANOVA (Kruskal-Wallis test). Data presented in mean±SEM. n=6 mice in each group.

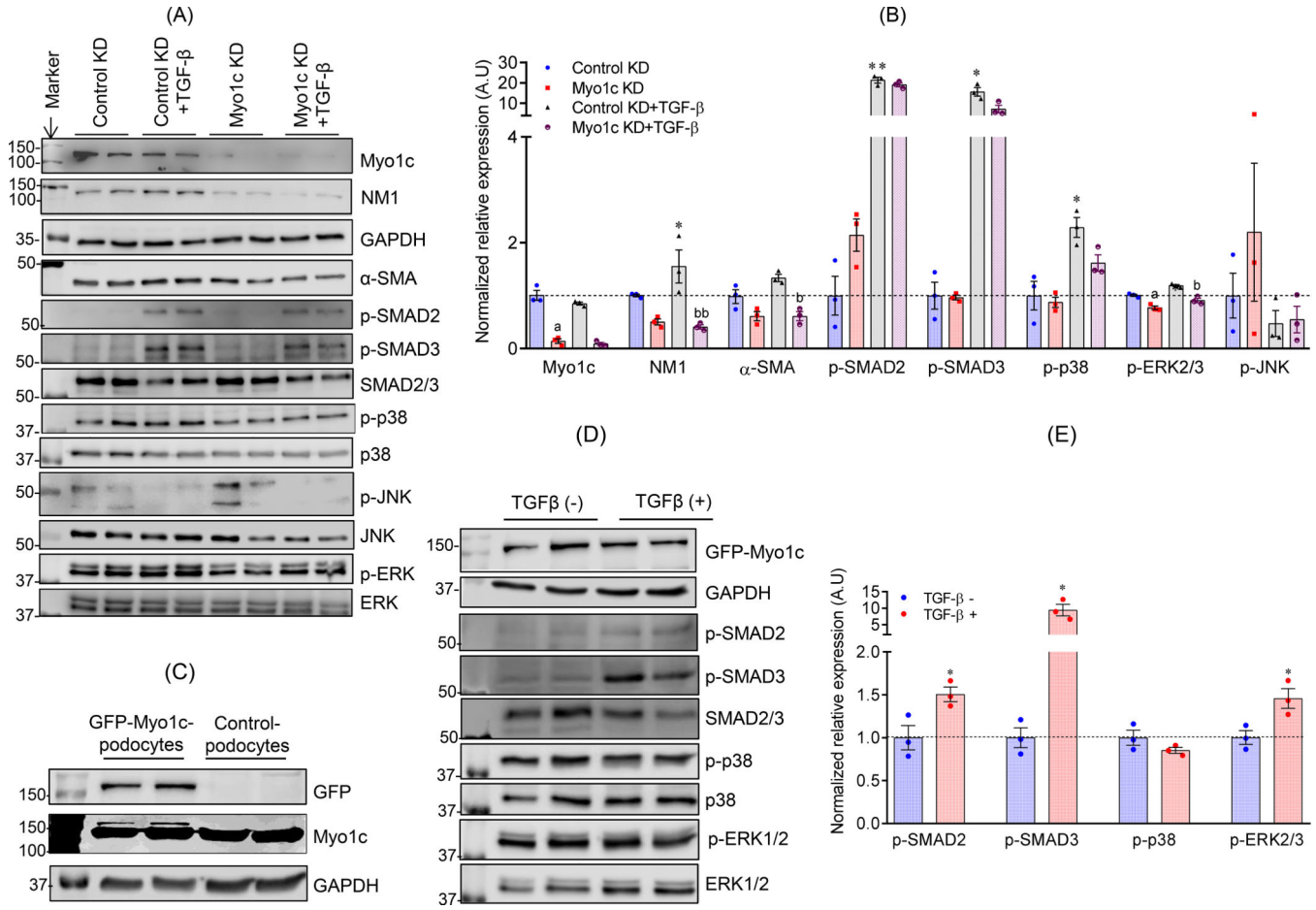


**Figure 6: TGF-β induced signaling is blunted in Myo1c-KD podocytes:**

(**A and B**) The signaling components of canonical and non-canonical TGF-β signaling pathways in control and Myo1c-KD podocytes were screened using western blotting. Quantitative analysis showed reduced phosphorylation of SMAD3, P38 and ERK1/2 proteins and reduced expression of α-SMA proteins in Myo1c-KD podocytes. All experiments were performed in triplicate. Data are presented in mean±SEM and p-values were calculated using one way ANOVA (Kruskal-Wallis test). ($^{a}P \leq 0.05$, control-KD vs Myo1c-KD; $^{bb}P \leq 0.001$, $^{b}P \leq 0.05$, control-KD TGFβ stimulated vs Myo1c-KD TGFβ stimulated; $^{**}P \leq 0.001$, $^{*}P \leq 0.05$, control-KD vs control-KD TGFβ stimulated). n=3 experimental replicates. (C) GFP-Myo1c over-expression was confirmed using western blot analysis. (D-E) TGF-β stimulation of in GFP-Myo1c over-expressed podocytes induced the expression of p-SMAD2, p-SMAD3 and p-ERK2/3. All experiments were performed in triplicate. Data are presented in mean±SEM and p-values were calculated using Mann-Whitney test (nonparametric test). $^{*}P \leq 0.05$, TGFβ- vs TGFβ+.

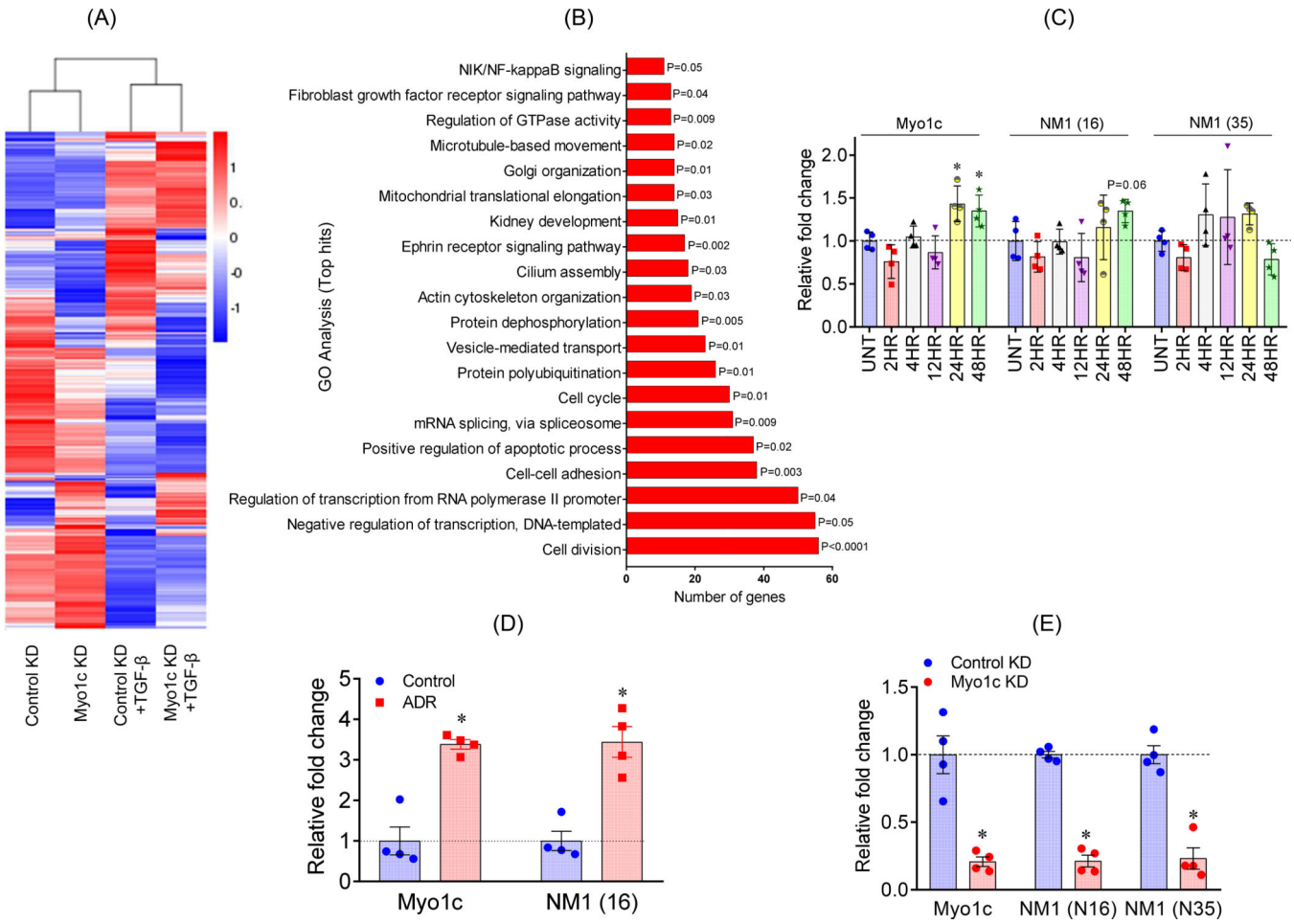


**Figure 7: Genes involved in TGF-β signaling were DE in Myo1c-KD podocytes.**

(**A**) The heat map from RNA-Seq data shows DEGs in Myo1c-KD podocytes in response to TGF-β +/− stimulation. (**B**) GO enrichment analysis showed multiple cellular events (presented as histograms) that were enriched in response to TGF-β stimulation of Myo1c-KD podocytes. $P \leq 0.05$, n=3 experimental replicates. (**C**) qPCR analysis showed upregulation of Myo1c and nuclear myosins isoforms NM(16) and NM(35) in response to TGF-β stimulation in a time dependent manner. *$P \leq 0.05$ vs untreated, one way ANOVA (Kruskal-Wallis test). n=3 experimental replicates. (**D**) Comparative qPCR analysis showed significant upregulation of Myo1c and nuclear myosin NM1(N16) in glomeruli isolated from adriamycin injured kidney. Data are presented as mean±SEM. *$P \leq 0.05$ vs. Myo1c$^{fl/fl}$, Mann-Whitney test (nonparametric test). n=3 mice glomeruli per group. **(E)** Myo1c-KD was performed using gene-specific shRNA and validated using qPCR. The qPCR analysis showed that expression of all Myo1c isoforms including, Myo1c, NM1(N16) and NM1(N35) was significantly reduced when compared to the control-KD cells. *$P \leq 0.05$ vs control-KD, Mann-Whitney test (nonparametric test). Data presented in mean±SEM. n=3 experimental repeats.

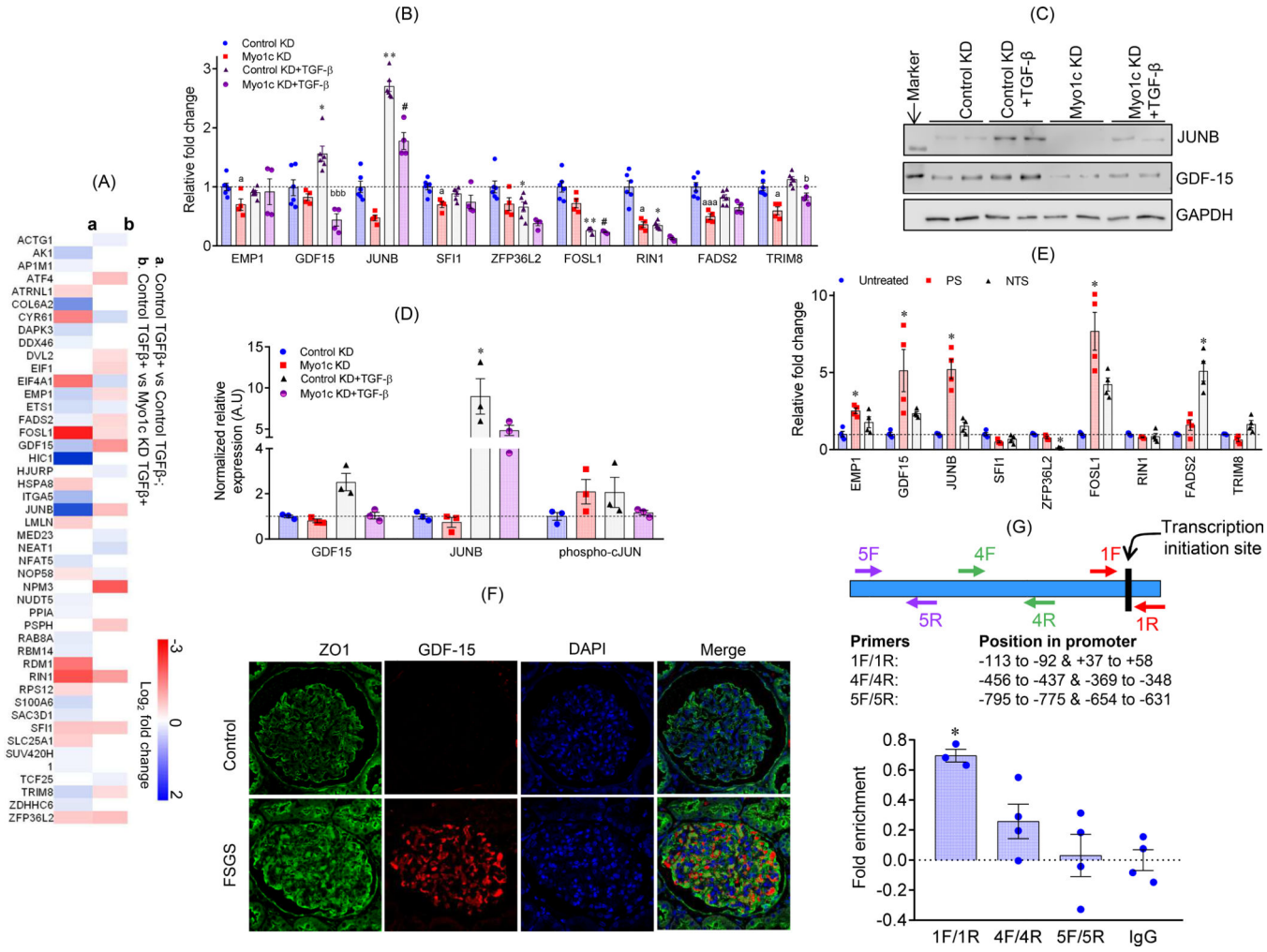


**Figure 8: NM1 associates with TGF-β responsive proteins GDF15 and JunB that are DE in Myo1c-KD podocytes.**

**(A)** The heat map shows genes that associate with Myo1c from the Chip-Seq analysis[47] and were DE upon stimulatiuon of podocytes with TGF-β. **(B)** qPCR analysis was performed of the genes that were upregulated upon TGF-β stimulation but were downregulated in Myo1c-KD podocytes. All experiments were performed in triplicate. Data are presented in mean ±SEM and p-values were calculated using one way ANOVA (Kruskal-Wallis test). ($^{aaa}P \leq 0.0001$, $^{a}P \leq 0.05$, control KD vs Myo1c-KD; $^{bbb}P \leq 0.0001$, $^{b}P \leq 0.05$, control-KD TGFβ stimulated vs Myo1c-KD TGFβ stimulated; $^{**}P \leq 0.001$, $^{*}P \leq 0.05$, control-KD vs control-KD TGFβ stimulated; $\#P \leq 0.05$, Myo1c-KD vs Myo1c-KD TGFβ stimulated). n=3 experimental replicates. **(C-D)** The protein expression of GDF-15 and JUNB was evaluated by western blotting using JunB and GDF-15 antibodies (**C**) and quantitatively assessed by densitometric analysis of the blots (**D**). All experiments were performed in triplicate. Data are presented in mean±SEM and p-values were calculated using one way ANOVA (Kruskal-Wallis test). ($^{*}P \leq 0.05$, control-KD vs control-KD TGFβ stimulated). **(E)** qPCR analysis to evaluate the expression of genes (that associate with NM1) in response to NTS and protamine sulphate-induced injuries in cultured human podocytes. All experiments were performed in triplicate. Data are presented in mean±SEM and p-values were calculated using one way ANOVA

(Kruskal-Wallis test).*$P \leq 0.05$, compare to untreated. (**F**) Parafilm embedded sections of kidneys from control and FSGS patients were immunostained with ZO1 (Green) and GDF-15 (Red) antibodies and DAPI (Blue). Expression of GDF- 15 was significantly upregulated in FSGS patients glomerulus. Scale bars: 20μm. **(G)** NM1 directly targets GDF-15 in podocytes. ChIP-qPCR analyses for NM1 occupancy of GDF-15 promoter in podocytes. Human podocytes were subjected to ChIP using anti- NM1 antibody/IgG antibody followed by qPCR of GDF-15 promoter regions. Schematic of the three sets of GDF-15 primers from the GDF-15 promoter are presented (upper panel). The bar-graph shows NM1 enriched region in the GDF15 promoter (F1/R1), which is proximal to the transcription initiation site (lower panel). Three independent experiments were performed with similar results. *P<0.05 Mann-Whitney test (nonparametric test) 1F/1R vs IgG. Data are presented as mean±SEM.

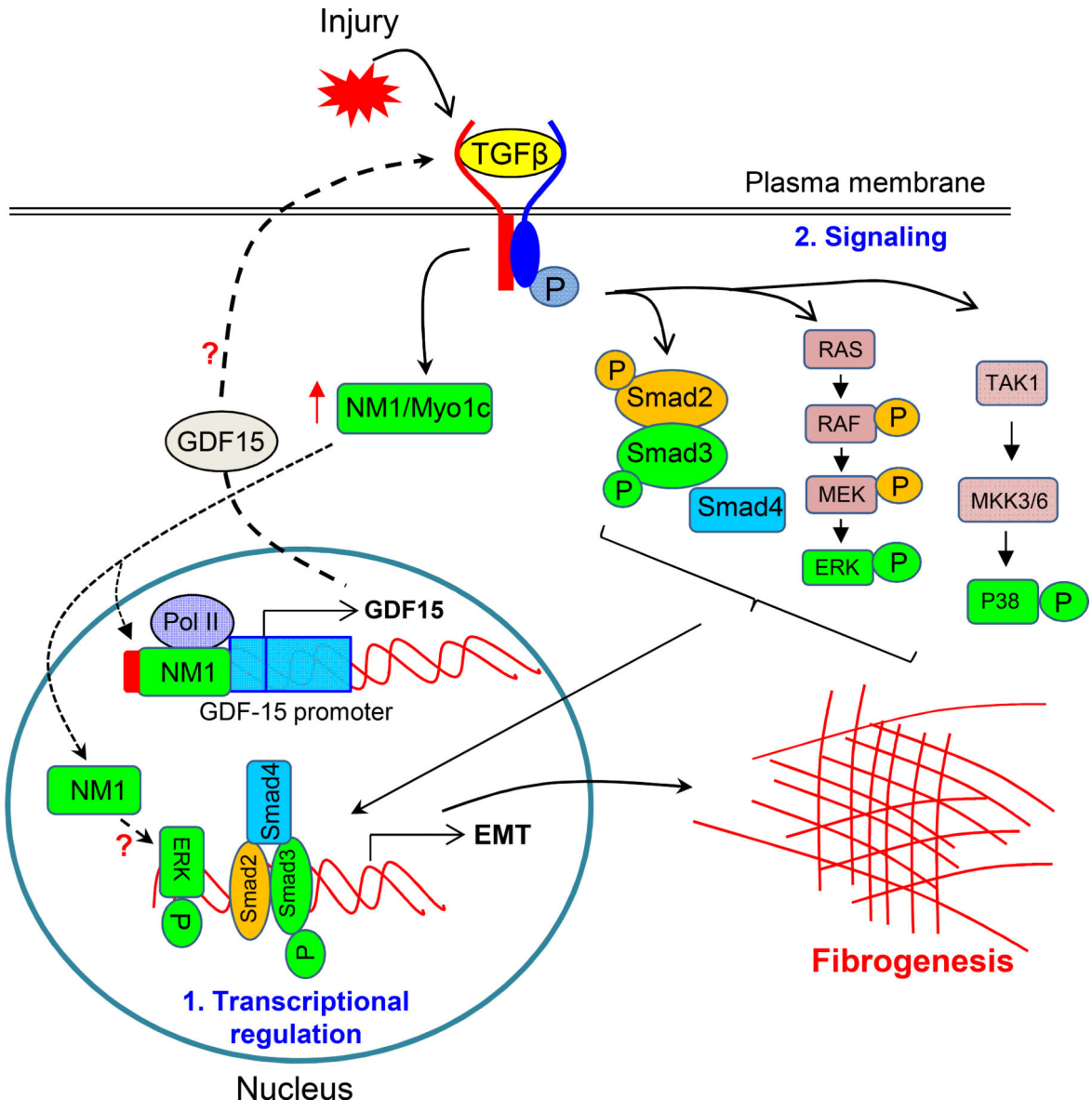


**Figure 9: Schematic description for the role of Myo1c in podocyte pathogenesis:**

Stimulation of TGF-β receptor either by injury or TGF-β induces canonical and non-canonical signaling cascades, along with NM1, which leads to the activation of TGF-β responsive genes including GDF15 in a NM1 dependent fashion. Since GDF15 can also act as a TGF-β receptor ligand, it can further regulate TGF-β signaling and fibrogenesis. Whether and how NM1 collaborates with Smads and non-Smads during TGF-β-induced EMT, needs further investigation.